11

Bipolar Junction Transistor Compact Models

11.1 Introduction

As described in Chapters 4 and 5, the *pn*-junctions are integral part of a MOSFET (metal-oxide-semiconductor field-effect transistor) device structure as the source and drain regions. Under the appropriate biasing condition of a MOSFET device, the source of the source-substrate *pn*-junction provides a steady supply of mobile carriers to form a conducting channel from the source to drain and the drain of the drain-substrate *pn*-junction collects the mobile carriers generating drain current. Two back-to-back *pn*-junctions form a bipolar junction transistor (BJT). BJTs are very often used in VLSI (very-large-scale-integrated) circuits. Therefore, a basic understanding of BJT modeling is necessary for engineers and researchers involved in device modeling. In this chapter, we present the basic but widely used BJT compact models for circuit CAD.

BJTs are active three-terminal devices and were the main active elements for ICs (integrated circuits) in the 1960s [1,2]. The areas of applications of BJTs include amplifiers, switches, high-power circuits, and high-speed logic circuits for high-speed computers. After the invention of bipolar transistors in 1947 [3], discrete BJTs were used to design circuits on printed circuit boards. In order to analyze the performance of BJTs, Ebers and Moll in 1954 reported a physics-based large signal BJT model, referred to as the *Ebers–Moll* or *EM* model [4]. The level 1 EM model, known as the EM1 model, is valid for the entire operating regime of BJTs from cutoff to active region. However, the application and accuracy of EM1 model are limited to evaluating the DC performance of the devices only due to several simplifying assumptions. In order to improve the modeling accuracy, EM1 model has been extended to EM2 and EM3 models for predicting the observed physical effects in BJTs including transient phenomena [5].

Though EM2 and EM3 models accurately predict most of the observed physical effects in BJTs, a more complete and unified physics-based BJT model was reported by Gummel and Poon in 1970 [6]. This model is known today as the *Spice Gummel–Poon* (SGP) model [7]. The SGP model uses an *integrated charge control* approach along with a very clear and standardized description of many observed effects in BJTs such as early effect [8], high current

roll-off [9], and carrier transit time [10]. Due to its simple yet physical model formulation, SGP model was the most popular BJT model until mid-1990s.

With the continued scaling of modern transistors, some second-order effects that are not considered by SGP model, such as substrate network, self-heating effects, and avalanche effects, became more and more important for accurate modeling of BJT ICs. A number of advanced BJT models have been introduced to model emerging and second-order physical effects to provide more precise simulation results [11]. These models include Vertical Bipolar Inter Company model [12], Most Exquisite Transistor Model [13], and High Current Model [14]. However, the SGP BJT model continued to be used in circuit CAD because of its simplicity. Therefore, in this chapter only EM and SGP models are described to provide readers the basic idea of BJT modeling. In model derivations, the emphasis is placed on the understanding of the effect being modeled along with the explanation of the required parameters. Thus, in this chapter, we use a systematic methodology to derive SGP compact BJT model, starting from the basic EM compact BJT model that provides an extremely useful understanding of the basic BJT operation.

11.2 Basic Features of BJTs

A silicon BJT structure is a sandwich of alternating type of doped silicon layers. Depending on the sequence of layers, two types of BJTs are manufactured: *npn* and *pnp*. An *npn*-BJT is a sequence of *n*-*p*-*n* layers whereas a *pnp*-BJT is a sequence of *p*-*n*-*p* layers. The *npn*-BJTs are most widely used in ICs with BJT technologies. Again, the sequence of layers may be used vertically to fabricate *vertical* BJTs or laterally referred to as the *lateral* BJTs. Figure 11.1 shows the basic structure of a vertical *npn*-BJT.

As shown in Figure 11.1b, the basic structure includes a heavily doped *n*+ emitter (E), a lightly doped *n*-epitaxial layer, a *p*-type base (B), and a heavily doped *n*+ buried collector (C) on a *p*-type substrate. The *p*+ isolation regions are used to isolate the adjacent devices in an IC chip. Typically, the isolation regions are reverse-biased *pn*-junctions; however, in advanced BJTs, trench isolation is used to increase the packing density of IC chips. The intrinsic device consists of *n*-*p*-*n* vertical cross section as shown in Figure 11.1b. The one-dimensional (1D) doping profile along the cutline from the surface of the active device is shown in Figure 11.1c. Figure 11.2 shows a typical layout of an IC *npn*-BJT.

Figure 11.1c shows that the base region is nonuniformly doped. As a result, a built-in electric field is set up to establish an equilibrium between the mobile carriers attempt to *diffuse* away from the high concentration region and mobile carriers pulled by the electric field (*drift*) of the fixed ionized donors (N_d^+) or acceptors (N_a^-) left behind by mobile carriers. The built-in electric field is obtained by setting: *diffusion* = *drift* (Equations 2.45 and 2.46).

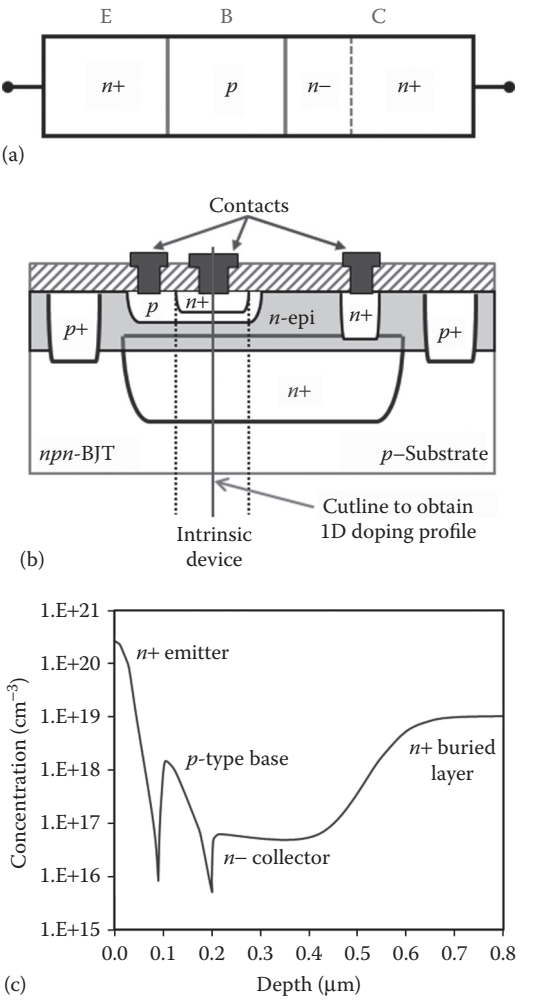

FIGURE 11.1
Basic feature of an *npn*-BJT: (a) an ideal structure showing an *n*+ emitter (E), a *p*-base (B), and *n*-*n*+ collector (C) regions; (b) 2D-cross section of a typical vertical *npn*-BJT used in ICs and (c) 1D doping profile along the cutline through the intrinsic device.

The basic BJT structure in Figure 11.1b shows that the BJTs also include a number of parasitic elements that must be accurately modeled in compact BJT models. The basic BJT structure has *base resistance*, r_b, mainly from the base contact to active area, a *collector resistance*, r_c (predominantly due to *n*-epitaxial layer as shown in Figure 11.1c), and an *emitter resistance*, r_e (typically, negligibly small). The *n*+ emitter and *p*-base junction includes an emitter-base (EB) junction capacitance (C_{jE}). The *n*– collector region adjacent to the base also includes a collector-base (CB) junction capacitance, C_{jC}. The advantages of the *n*-layer include a reduction in C_{jC}, an improvement in the CB breakdown

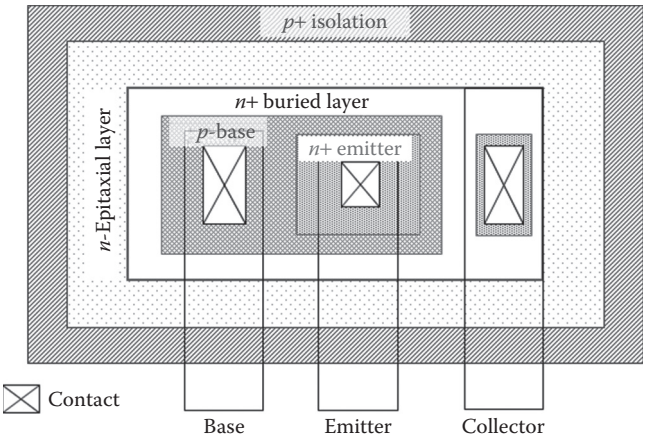

FIGURE 11.2
Typical layout of a vertical *npn*-BJT device shown in Figure 11.1(b) used for fabrication in an IC chip.

voltage BV_{CB}, and a decrease in the base-width modulation by the collector voltage at a cost of collector terminal series resistance R_C.

11.3 Basic Operation of BJTs

In order to describe the basic operation of BJTs, let us consider the structure and biasing condition shown in Figure 11.3.

In a typical *npn*-BJT operation, an external potential, V_{BE} (≈ 0.7 V), is applied across the EB-junction to forward bias it, as shown in Figure 11.3. *Electrons* are injected into the base by the emitter. (*Also, holes are injected into the emitter but their numbers are much lower because of the relative values of* N_a and N_d.) If the effective base width $W_B << L_n$ (electron diffusion length) in the base, most of the injected electrons get into the collector without recombining. A few do recombine; the *holes* necessary for this are supplied as the base current, I_B. The electrons reaching the collector are collected across the CB-junction depletion region (X_{dCB}) under the reverse bias CB-junction, V_{BC}, and generates collector current, I_C. The carrier transport process is shown in Figure 11.4a and the circuit representation of an *npn*-BJT is shown in Figure 11.4b. In Figure 11.4, I_E represents the emitter current. Conventionally, the current flowing into the device terminal is defined as positive.

Since most of the injected electrons reach the collector, only a few holes are injected into the emitter; therefore, $I_B << I_C$. As a result, the BJT device has a substantial current gain (I_C/I_B). *Note that the built-in electric field across the base also aids electron transport from E to C.*

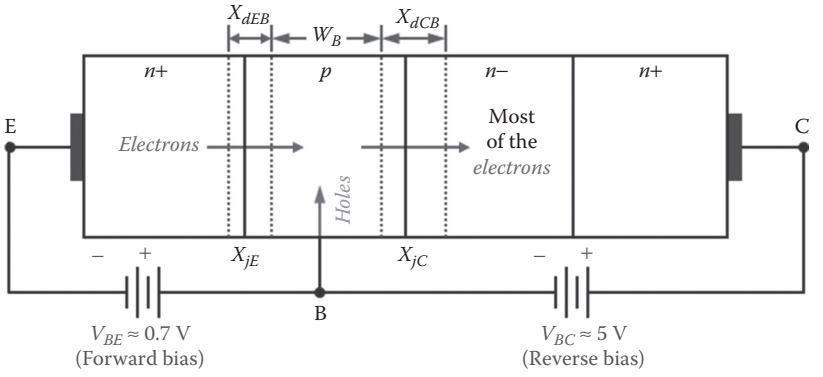

FIGURE 11.3
A typical biasing condition of an *npn*-BJT: the EB-junction is forward biased and CB-junction is reverse biased; W_B is the effective width of the neutral base region; X_{jE} and X_{jC} are the EB and CB metallurgical junctions, respectively; and X_{dEB} and X_{dCB} are the EB and CB depletion regions, respectively.

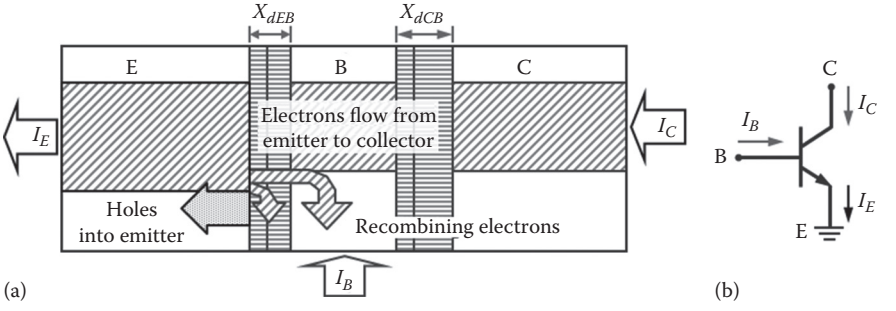

FIGURE 11.4
An *npn*-BJT operation: (a) carrier transport under the forward active mode of operation; the base-emitter junction is forward biased and base-collector junction is reverse biased and (b) circuit representation. I_C, I_B, and I_E are the collector, base, and emitter terminal currents, respectively.

11.4 Mode of Operations of BJTs

In order to develop compact BJT models for circuit CAD, let us define the operation regions of BJT devices. Depending on the biasing conditions, we can define four different modes of BJT operations as shown in Figure 11.5 for an *npn*-BJT device.

1. *Forward active* or *normal* mode: EB-junction is *forward* biased; and CB-junction is *reverse* biased. In this case, the collector current $I_C = \beta_F I_B$, where β_F is the forward current gain;

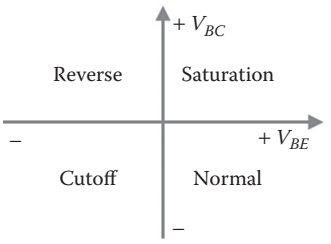

FIGURE 11.5
Four different regions of operation of an *npn*-BJT device depending on the biasing conditions: normal active, saturation, inverse active, and cutoff; where V_{BE} and V_{BC} are the EB-junction voltage and CB-junction voltage, respectively.

2. *Reverse active* mode: EB-junction is *reverse* biased and CB-junction is *forward* biased. In this case, the reverse current at emitter terminal $I_E = \beta_R I_B$, where β_R is the reverse current gain ≈ 1;
3. *Saturation*: both EB- and CB-junctions are forward biased;
4. *Cutoff*: both EB- and CB-junctions are reverse biased.

Similarly, we can define the different regions of a *pnp*-BJT operation by appropriately changing the sign of V_{BE} and V_{CE}.

Figure 11.6 shows the device characteristics of both *npn*- and *pnp*-BJTs showing different regions of operation. In order to analyze the device characteristics in Figure 11.6, let us consider an *npn*-BJT in the normal active mode of operation. From Figure 11.4b we can show that the collector–emitter voltage

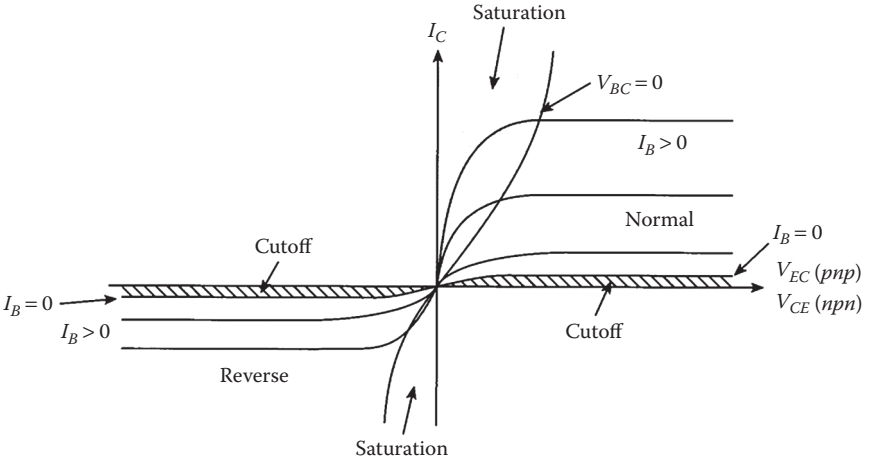

FIGURE 11.6
Collector current versus collector–emitter voltage with base current as the third parameter for both *npn*- and *pnp*-BJTs; plot shows all four regions of device operation, depending on the applied collector–emitter voltage.

$V_{CE} = V_{BE} - V_{BC}$. Therefore, at $V_{CE} = 0$, and $V_{BE} \geq \phi_{BE}$, $V_{BE} = V_{BC}$, where ϕ_{BE} is the built-in-potential of EB-junction (Equation 2.109). Under this condition, both the EB- and CB-junctions are forward biased, resulting in a decrease in the barrier height for electrons at both EB- and CB-junctions (Equation 2.100). Consequently, both emitter and collector junctions inject electrons into the base. Under this biasing condition, the electric field does not favor transport of electrons to the collector (or emitter) terminal and $I_C = 0$ and the device is in *saturation*. Thus, for $0 \leq V_{CE} < V_{BE}$, the *npn*-BJT operates in the saturation regime since both the EB- and CB-junctions are forward biased. As V_{CE} increases from $V_{CE} = 0$ due to the increasing collector supply voltage V_{CC}, V_{BC} gradually becomes less forward biased and the CB-junction barrier height gradually increases. Therefore, electron injection from the emitter to base dominates over that from the collector to base and I_C increases with the increase in V_{CE} as shown in Figure 11.6. At $V_{CE} = V_{BE}$ (or, $V_{BC} = 0$), the *npn*-BJT is at the onset of transition from the saturation region to the *normal active* mode of operation, and for $V_{CE} > V_{BE}$, the *npn*-BJT operates in the normal active *linear regime*. Therefore, the loci of the point $V_{CE} = V_{BE}$ on I_C–V_{CE} plot separates the saturation and linear regions of BJTs as shown in Figure 11.6.

Again, when $V_{CE} < 0$, both the EB- and CB-junctions are reverse biased. This increases the potential barrier height of electrons for both the *pn*-junctions and there is no electron injection from the emitter or collector to the base region of the transistor resulting in $I_C \approx 0$. Under this condition, the device operates in the *cutoff* region as shown in Figure 11.6. Similarly, we can explain the *pnp*-BJT characteristics. Note the difference between the MOSFET and BJT linear and saturation region of operations (Section 4.4.4.1).

11.5 Compact BJT Model

In order to develop a complete BJT model for circuit CAD, we first develop the basic DC model using the Ebers–Moll formulation and then include the different parasitic elements of the BJT structure and physical effects.

11.5.1 Basic DC Model: EM1

In order to derive a basic BJT current model, let us consider an *npn*-BJT device shown in Figure 11.7. As seen from Figure 11.7, a BJT structure can be considered as two back-to-back *pn*-junctions. For the simplicity of basic model formulation, we assume that all the parasitic elements such as series resistances and junction capacitances are negligibly small.

Now, let us assume that the *npn*-BJT is biased in the normal active mode of operation ($V_{BE} \geq \phi_{BE}$ and $V_{BC} < 0$). Then when the EB *pn*-junction is forward biased, a forward current I_F flows through the EB *pn*-junction and a current $\alpha_F I_F$ flows across the CB *pn*-junction, where α_F is the forward current gain

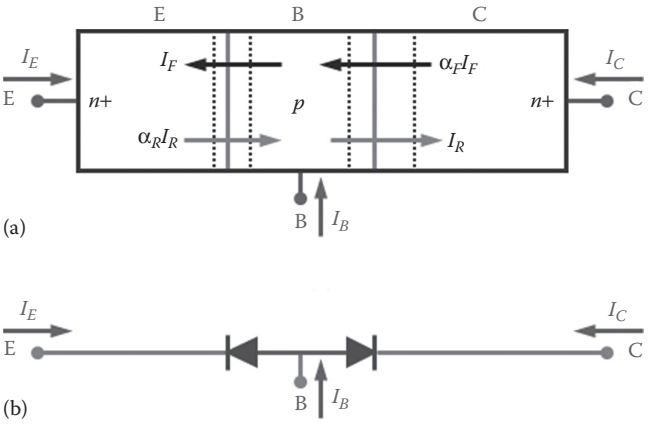

FIGURE 11.7
An ideal *npn*-BJT structure used to derive the basic Ebers–Moll model: (a) the transistor configuration with carrier injection due to the applied biases and (b) the *npn*-BJT structure represented by two back-to-back *pn*-junctions.

given by I_C/I_E for $V_{BE} > 0$. Similarly, for the reverse-biased CB *pn*-junction, a reverse current, I_R, flows through the CB *pn*-junction and a current, $\alpha_R I_R$, flows through the EB *pn*-junction, where α_R is the reverse current gain and is given by I_E/I_C for $V_{BC} < 0$. Then from Figure 11.7a, the terminal currents are given by

$$\begin{aligned} I_E &= -I_F + \alpha_R I_R \\ I_C &= \alpha_F I_F - I_R \end{aligned} \tag{11.1}$$

The physical concept described in Figure 11.7 can be represented by an equivalent circuit shown in Figure 11.8.

Figure 11.8 represents the basic *npn*-BJT model for circuit CAD and is known as the basic Ebers–Moll or EM1 BJT model. From Figure 11.8 the terminal currents are given by

$$I_E = -I_F + \alpha_R I_R \tag{11.2}$$

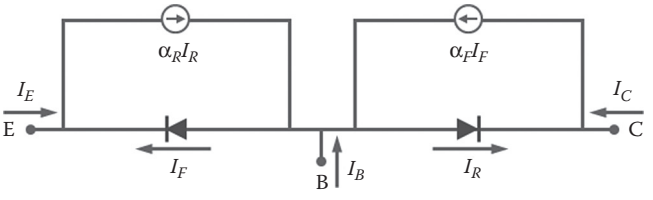

FIGURE 11.8
The basic Ebers–Moll model for an *npn*-BJT: the basic model is obtained by considering two back-to-back *pn*-junctions. Here, $\alpha_F I_F$ and $\alpha_R I_R$ are the current sources at the CB and EB *pn*-junctions, respectively.

$$I_C = \alpha_F I_F - I_R \tag{11.3}$$

$$I_B = I_F - \alpha_R I_R + I_R - \alpha_F I_F = (1-\alpha_F) I_F + (1-\alpha_R) I_R \tag{11.4}$$

From Equation 2.119, we can write the expression for the forward electron current flow through the EB *pn*-junction as

$$I_F = I_{nE} = I_{ES}\left[\exp\left(\frac{V_{BE}}{v_{kT}}\right)-1\right] \tag{11.5}$$

and, the reverse electron current flow through the CB *pn*-junction as

$$I_R = I_{nC} = I_{CS}\left[\exp\left(\frac{V_{BC}}{v_{kT}}\right)-1\right] \tag{11.6}$$

where:

I_{ES} and I_{CS} are the saturation currents of the EB and CB *pn*-junctions, respectively

V_{BE} and V_{BC} are the applied voltages at the EB and CB *pn*-junctions, respectively

Then from Equations 11.2 through 11.6, the terminal currents for an *npn*-BJT can be shown as

$$I_E = -I_{ES}\left[\exp\left(\frac{V_{BE}}{v_{kT}}\right)-1\right] + \alpha_R I_{CS}\left[\exp\left(\frac{V_{BC}}{v_{kT}}\right)-1\right] \tag{11.7}$$

And,

$$I_C = \alpha_F I_{ES}\left[\exp\left(\frac{V_{BE}}{v_{kT}}\right)-1\right] - I_{CS}\left[\exp\left(\frac{V_{BC}}{v_{kT}}\right)-1\right] \tag{11.8}$$

From the reciprocity property $\alpha_F I_{ES} = \alpha_R I_{CS} \equiv I_S$, where I_S is the reverse saturation current of an *npn*-BJT device, so we can express Equations 11.7 and 11.8 as

$$I_E = -\frac{I_S}{\alpha_F}\left[\exp\left(\frac{V_{BE}}{v_{kT}}\right)-1\right] + I_S\left[\exp\left(\frac{V_{BC}}{v_{kT}}\right)-1\right] \tag{11.9}$$

And,

$$I_C = I_S\left[\exp\left(\frac{V_{BE}}{v_{kT}}\right)-1\right] - \frac{I_S}{\alpha_R}\left[\exp\left(\frac{V_{BC}}{v_{kT}}\right)-1\right] \tag{11.10}$$

Again, using $\alpha_F = I_C/I_E$ and $\alpha_R = I_E/I_C$, we can show that the forward current gain $\beta_F = I_C/I_B$ and the reverse current gain $\beta_R = I_B/I_C$ are given by

$$\beta_F = \frac{\alpha_F}{(1-\alpha_F)}$$
$$\beta_R = \frac{\alpha_R}{(1-\alpha_R)} \tag{11.11}$$

From Equation 2.121, the temperature dependence of the saturation current I_S at any ambient temperature T with respect to reference temperature T_{NOM} is given by

$$I_S(T) = I_S(T_{NOM})\left(\frac{T}{T_{NOM}}\right)^3 \exp\left[\frac{E_g(T_{NOM})}{kT_{NOM}} - \frac{E_g(T)}{kT_{NOM}}\right] \tag{11.12}$$

where:

E_g is the energy gap of the silicon substrate

The BJT current model obtained in Equations 11.9 and 11.10 are known as the *injection version* of EM1 model.

To further simplify the model, we define the reference current source I_{CC} due to the forward injection at EB *pn*-junction by applied voltage V_{BE} and source current I_{EC} due to the reverse injection at CB *pn*-junction by applied bias V_{BC}. Then from Equation 2.119, we get

$$I_{CC} = I_S\left[\exp\left(\frac{V_{BE}}{v_{kT}}\right) - 1\right]$$
$$I_{EC} = I_S\left[\exp\left(\frac{V_{BC}}{v_{kT}}\right) - 1\right] \tag{11.13}$$

Using Equation 11.13, the model Equations 11.9 and 11.10 can be written as

$$I_E = \left(-\frac{1}{\alpha_F}\right) I_{CC} + I_{EC} \tag{11.14}$$

$$I_C = I_{CC} - \frac{1}{\alpha_R} I_{EC} \tag{11.15}$$

And, from Kirchhoff's current law, the base current $I_B = -(I_E + I_C)$ is given by

$$I_B = \left(\frac{1}{\alpha_F} - 1\right) I_{CC} + \left(\frac{1}{\alpha_R} - 1\right) I_{EC} \tag{11.16}$$

Equations 11.14 through 11.16 present the *npn*-BJT terminal currents with reference to source currents I_{CC} and I_{EC} given by Equation 11.13. This is referred

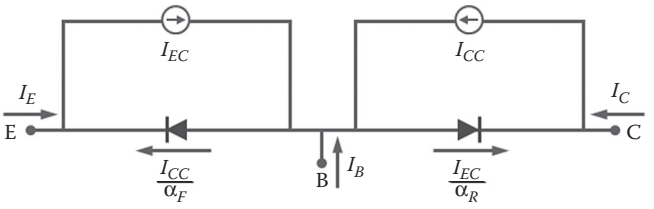

FIGURE 11.9
The transport version of the basic Ebers–Moll model for an *npn*-BJT; the model is derived with reference to source currents I_{CC} and I_{EC}.

to as the EM1 *transport model* and the corresponding equivalent circuit is shown in Figure 11.9.

We can further simplify the model by adding and subtracting I_{CC} on the right-hand side of Equation 11.14 to get

$$I_E = \left(1 - \frac{1}{\alpha_F}\right) I_{CC} - \left(I_{CC} - I_{EC}\right) = -\frac{I_{CC}}{\beta_F} - I_{CT} \tag{11.17}$$

Similarly, by adding and subtracting I_{EC} on the right-hand side of Equation 11.15, we get

$$I_C = \left(I_{CC} - I_{EC}\right) - \left(\frac{1}{\alpha_R} - 1\right) I_{EC} = I_{CT} - \frac{I_{EC}}{\beta_R} \tag{11.18}$$

where $I_{CT} = (I_{CC} - I_{EC})$; in Equations 11.17 and 11.18, we have used Equation 11.11 to replace α_F and α_R by β_F and β_R, respectively. Now, from Equation 11.13, the current source I_{CT} can be expressed as

$$I_{CT} = \left(I_{CC} - I_{EC}\right) = I_S \left\{ \left[\exp\left(\frac{V_{BE}}{v_{kT}}\right) - 1 \right] - \left[\exp\left(\frac{V_{BC}}{v_{kT}}\right) - 1 \right] \right\} \tag{11.19}$$

Note that I_{CT} models the current source in a BJT and describes the current flow through the device in the normal active model of operation. With reference to Equations 11.17 and 11.18, the equivalent circuit for the final version of EM1 transport model defined as the *nonlinear hybrid-*π model is shown in Figure 11.10

Thus, the terminal currents of the *transport version* of the basic EM1 model are given by

$$\begin{aligned} I_E &= -\frac{I_{CC}}{\beta_F} - I_{CT} \\ I_C &= I_{CT} - \frac{I_{EC}}{\beta_R} \\ I_B &= \frac{I_{CC}}{\beta_F} + \frac{I_{EC}}{\beta_R} \end{aligned} \tag{11.20}$$

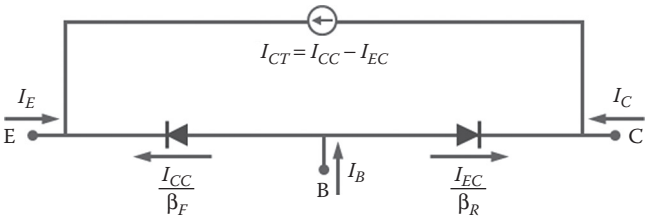

FIGURE 11.10
The nonlinear hybrid-π EM1 model for an *npn*-BJT; the model is derived with reference to the source current I_{CT}.

The currents I_{CT}, I_{CC}, and I_{EC} in the basic model (Equation 11.20) depend on I_S that depends on ambient temperature T_{NOM} and energy gap E_g, given by Equation 11.12. Thus, the EM1 transport model can be characterized by five model parameters: β_F, β_R, I_S, T_{NOM}, and E_g. The basic EM1 model can be used to analyze the performance of BJTs over the entire operating regimes at any temperature by five parameters only.

11.5.1.1 Linear Hybrid-π Small Signal Model

For small signal analysis, the total current (i_C) and total BE-junction voltage (v_{BE}) are denoted by their DC values and an incremental (small signal) quantity as

$$i_C = I_C + i_c$$
$$\text{and} \tag{11.21}$$
$$v_{BE} = V_{BE} + v_{be}$$

where:
i_c and v_{be} are the small signal collector current and EB *pn*-junction voltage, respectively

The ratio of i_c and v_{be} at a given DC bias point (V_{BE}, I_C) is defined as the *transconductance* g_m and is given by

$$g_m = \left.\frac{i_c}{v_{be}}\right|_{(V_{BE}, I_C)} = \left.\frac{\partial i_C}{\partial v_{BE}}\right|_{(V_{BE}, I_C)} \tag{11.22}$$

The incremental change in i_C due to an increment in v_{BE} is represented by a voltage-controlled current source. From Equation 11.19, the collector current in the forward active region is given by

$$i_C \cong I_S \exp\frac{v_{BE}}{v_{kT}} \tag{11.23}$$

Now, using Equation 11.23 in Equation 11.22, we get

$$g_m = \frac{I_S}{v_{kT}} \exp\frac{v_{BE}}{v_{kT}} = \frac{I_C}{v_{kT}} \tag{11.24}$$

The transconductance connects the BE-junction terminal potential with the collector current and is the central element in the small signal model. To establish a relation of the current source in small signal model, let us write the exact expression for the collector current as a function of BE-junction voltage

$$i_C = I_C + i_c = I_S \exp\left[\frac{(V_{BE} + v_{be})}{v_{kT}}\right] = I_C \exp\left(\frac{v_{be}}{v_{kT}}\right) \tag{11.25}$$

Since $v_{be} << v_{kT}$, then by series expansion of Equation 11.25 and neglecting the higher order terms, we get

$$I_C + i_c = I_C \exp\left(\frac{v_{be}}{v_{kT}}\right) = I_C\left(1 + \frac{v_{be}}{v_{kT}} + \cdots\right) \tag{11.26}$$

From Equations 11.24 and 11.26, we get the expression for small signal current source as

$$i_c \cong g_m v_{be} \tag{11.27}$$

Input resistance: In order to find the small signal resistor that models the incremental base current due to v_{be}, we define the small signal forward current gain at the operating point $Q = (V_{BE}, I_C)$ as

$$\beta_F = \left.\frac{\partial i_C}{\partial i_B}\right|_Q \tag{11.28}$$

The small signal current gain may vary with the operating point; however, for the first-order analysis we assume the small signal current gain (β_o) at Q is equal to the forward current gain given by Equation 11.28. Then the input resistance is defined by

$$\frac{1}{r_\pi} = \left.\frac{\partial i_B}{\partial v_{BE}}\right|_Q \tag{11.29}$$

Applying the chain rule and substituting the small signal current gain from Equation 11.27, we find that

$$\frac{1}{r_\pi} = \left.\frac{\partial i_B}{\partial v_{BE}}\right|_Q = \left.\frac{\partial i_B}{\partial i_C}\right|_Q \left.\frac{\partial i_C}{\partial v_{BE}}\right|_Q = \frac{g_m}{\beta_F} \tag{11.30}$$

where we identified the transconductance g_m from Equation 11.22. Substituting for g_m from Equation 11.24 at the operating point Q, we find the input resistance is

$$r_\pi = \frac{\beta_F v_{kT}}{I_C} = \frac{\beta_F}{g_m} \tag{11.31}$$

From Equation 11.31, it is obvious that the input resistance of BJTs is inversely proportional to the DC collector current I_C and directly proportional to the small signal current gain β_F.

Output resistance: In the normal active mode of operation, the CB-junction is reverse biased. Therefore, the output resistance of the reverse-biased *pn*-junction is defined by

$$\frac{1}{r_o} = \left.\frac{\partial i_C}{\partial v_{CE}}\right|_Q \equiv g_o \tag{11.32}$$

where:

g_o is the output conductance of the device

In EM1 BJT model, $r_o \equiv r_\mu$ is assumed to be extremely large, that is, open circuit. Therefore, the small signal equivalent circuit of the basic BJT model can be shown as in Figure 11.11

The basic EM1 model is fairly accurate only for modeling the DC characteristics of BJTs at any ambient temperature, *T*. However, the model cannot be used for transient analysis since in deriving the EM1 model we have neglected the effect of parasitic elements. In the next section, we will update

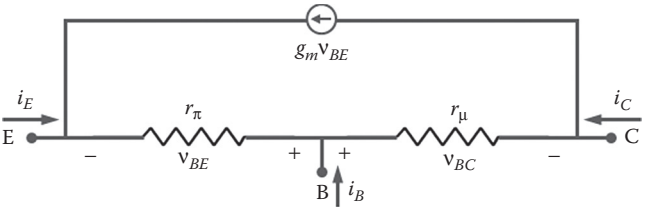

FIGURE 11.11
Small signal model of an *npn*-BJT derived from the basic transport version of the model shown in Figure 11.10.

the basic model by including the parasitic resistances and the capacitances to enable transient analysis and improve DC modeling accuracy. This updated EM1 model is often referred to as the EM2 BJT model and is described in the following section.

11.5.2 Enhancement of the Basic Model

11.5.2.1 Modeling Parasitic Circuit Elements

The basic BJT model is extended to improve DC modeling accuracy and enable transient simulation by including parasitic circuit elements in BJT modeling. The parasitic elements in BJTs include (1) the bulk-resistances r_e, r_b, and r_c of the neutral emitter, base, and collector regions, respectively; (2) EB-junction diffusion capacitance C_{DE} due to the diffusion of injected carriers from the emitter to the collector through the base and CB-junction diffusion capacitance C_{DC} due to the diffusion of injected carriers from the collector to the emitter through the base; and (3) junction capacitances C_{jE}, C_{jC}, and C_{sub} of the EB, CB, and collector-substrate *pn*-junctions, respectively. Different parasitic elements (except C_{DE} and C_{DC}) are shown in Figure 11.12a. The enhanced model is sometimes referred to as the EM2 model.

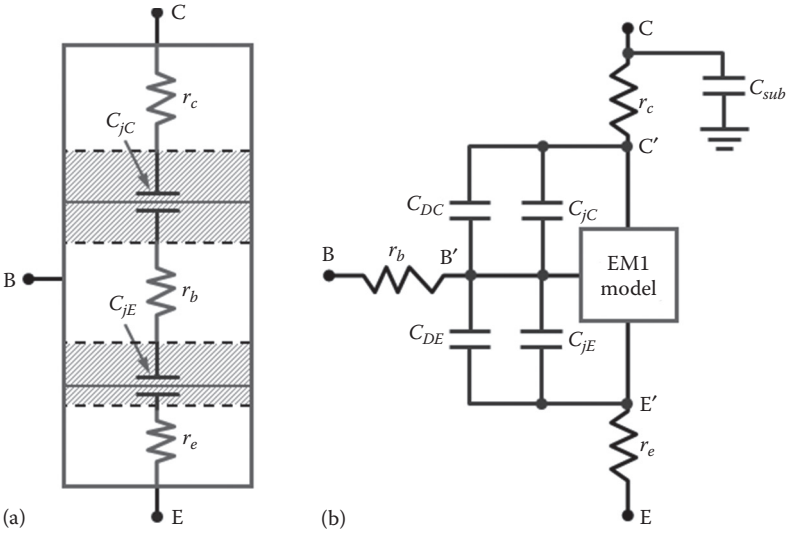

FIGURE 11.12
The equivalent circuit of an enhanced vertical *npn*-BJT model: (a) parasitic elements in the ideal BJT structure and (b) addition of parasitic resistors and capacitors in the basic model to improve the DC modeling accuracy and transient modeling capability; E′, B′, and C′ are the internal nodes of the emitter, base, and collector of the transistor, respectively; and C_{sub} is the collector-substrate *pn*-junction capacitance of the vertical *npn*-BJT structure.

With the consideration of the bulk resistances, the internal and terminal voltages are different due to the ohmic drop across the neutral bulk regions. Thus, including the ohmic bulk-resistors to improve DC characteristics and capacitors to model the charge storage effects in the basic model, we get the equivalent circuit of the model shown in Figure 11.12b.

Figure 11.12b shows the equivalent circuit of a vertical *npn*-BJT model to include its intrinsic parasitic resistive and capacitive elements in the basic EM1 model block. Replacing the EM1 model block in Figure 11.12b by the equivalent circuit of EM1 transport model shown in Figure 11.10, we get the revised compact *npn*-BJT model to account for the series resistance and charge storage effects in BJTs is shown in Figure 11.13.

From Equation 11.13, we can write the expressions for the currents flowing through the EB and CB *pn*-junctions in Figure 11.13 as

$$\frac{I_{CC}}{\beta_F} = \frac{I_S}{\beta_F}\left[\exp\left(\frac{V_{B'E'}}{v_{kT}}\right) - 1\right]$$
$$\frac{I_{EC}}{\beta_R} = \frac{I_S}{\beta_R}\left[\exp\left(\frac{V_{B'C'}}{v_{kT}}\right) - 1\right] \tag{11.33}$$

where:

$V_{B'E'} = V_{BE} - I_E r_e$ and $V_{B'C'} = V_{BC} - I_C r_c$ are the EB and CB internal voltages, respectively, as shown in Figures 11.13 and 11.14

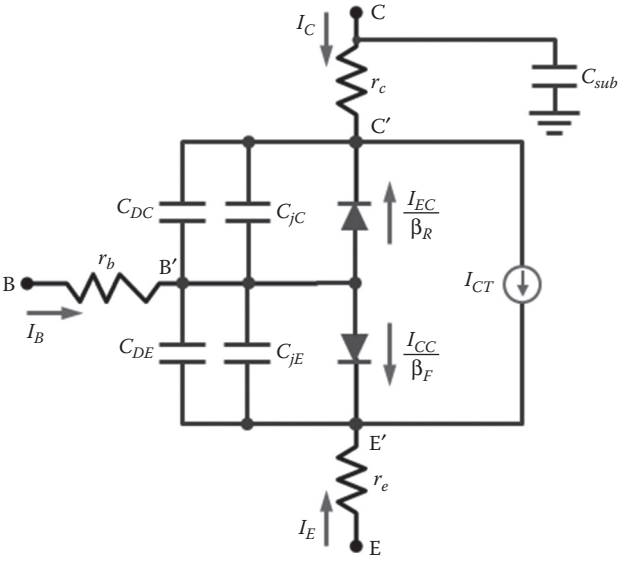

FIGURE 11.13
The equivalent circuit of the enhanced vertical *npn*-BJT model: parasitic resistances and capacitances are included to improve predictability of the simulation results.

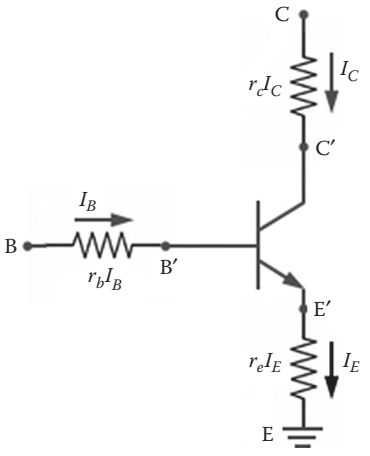

FIGURE 11.14
The parasitic series resistances on a typical *npn*-BJT device causing ohmic voltage drop at the respective neutral regions of the device.

Let us look at the impact of parasitic resistors shown in Figures 11.13 and 11.14 on the characteristics of a typical BJT device.

- *Effect of ohmic bulk collector resistor,* r_c: The collector series resistance r_c decreases the slope of I_C versus V_{CE} characteristics in the saturation region of BJT operation and improves the accuracy of modeling DC device characteristics as shown in Figure 11.15. Figure 11.15 shows (I_C, I_B) as a function of V_{CE} of an *npn*-BJT. As shown in Figure 11.15, r_c increases the transition voltage $V_{CE,sat}$ of BJTs. The typical value of r_c of modern IC BJTs is about 200 ohm.

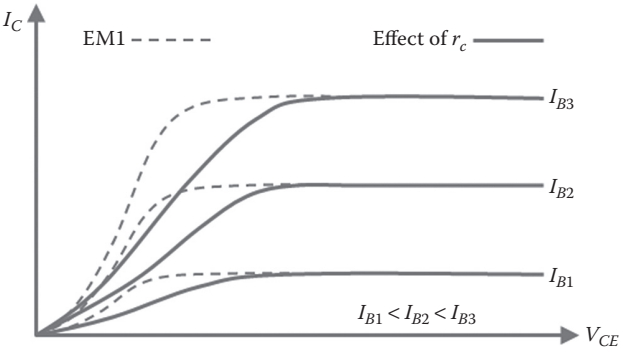

FIGURE 11.15
The effect of collector series resistance on the BJT device characteristics is to increase the saturation to linear region transition voltage $V_{CE,sat}$ of BJTs.

- *Effect of emitter series resistance,* r_e: The ohmic drop due to r_e reduces the EB-junction potential V_{BE} by a factor of r_eI_E by the emitter current I_E so that

$$\Delta V_{BE} = I_E r_e = \left(I_C + I_B\right) r_e = I_B\left(1+\beta_F\right) r_e \tag{11.34}$$

  From Equation 11.34 we find that r_e results in an equivalent base resistance of $(1 + \beta_F)r_e$. Since the emitter region is heavily doped ($\geq 1 \times 10^{19}$ cm^{-3}), r_e is negligibly small. However, due to the contact resistance at the emitter terminal and since $\beta_F >> 1$, a typical value of r_e is about 5 ohm is obtained. Therefore, though the value of r_e is very small, it affects both I_C and I_B due to the voltage drop $\Delta V_{BE} = I_B\left(1+\beta_F\right) r_e$ as shown in Figure 11.16.
- *Effect of base series resistance,* r_b: The base series resistance also reduces the EB-junction potential V_{BE} by a factor of r_bI_B as shown in Figure 11.16. It effects the small signal and transient response of BJTs and difficult to measure accurately due to the dependence on r_e and operating point as shown in Figure 11.16.
- *Effect of junction capacitances*: The EB- and CB-junction capacitances per unit area C_{jE} and C_{jC}, respectively, model the incremental fixed charges stored in the space EB- and CB-junction space-charge regions of BJTs due to the applied bias V_{BE} and V_{BC}, respectively. From Equation 2.139, we can write the expression for EB *pn*-junction capacitance in terms of internal node voltages as

$$C_{JE}\left(V_{BE}\right) = \frac{C_{jE0}}{\left[1+\left(V_{B'E'}/\phi_{BE}\right)\right]^{m_{jE}}} \tag{11.35}$$

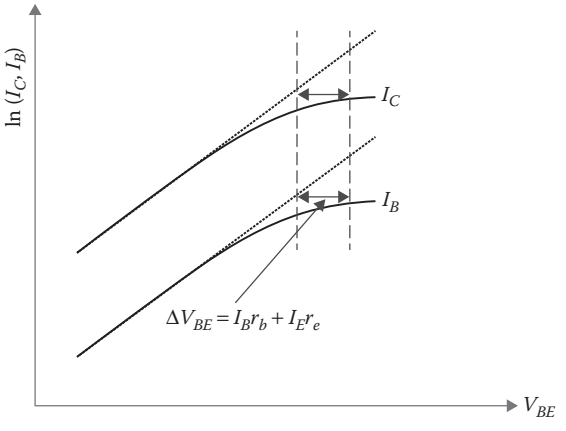

FIGURE 11.16
The saturation of I_C and I_B at higher values of V_{BE} due to the ohmic voltage drops at the base and emitter series resistances of BJT devices.

where:

C_{jE0} is the EB-junction capacitance per unit area at $V_{B'E'} = 0$
m_{jE} is the doping gradient coefficient
ϕ_{BE} is the EB-junction built-in potential that depends on the base doping concentration N_B and emitter doping concentration, N_E

We can show from Equation 2.109

$$\phi_{BE} = v_{kT} \ln\left(\frac{N_B N_E}{n_i^2}\right) \tag{11.36}$$

where:

$N_B = N_a$ (acceptor concentration)
$N_E = N_d$ (donor concentration) for *npn*-BJTs.

Similarly, the CB-junction capacitance due to V_{BC} is given by

$$C_{JC}\left(V_{BC}\right) = \frac{C_{jC0}}{\left[1 + \left(V_{B'C'}/\phi_{BC}\right)\right]^{m_{jC}}} \tag{11.37}$$

where:

C_{jC0} is the CB-junction capacitance per unit area at $V_{B'C'} = 0$
ϕ_{BC} is the CB built-in potential that depends on base doping concentration N_B and collector doping concentration, N_C

and is given by

$$\phi_{BC} = v_{kT} \ln\left(\frac{N_B N_C}{n_i^2}\right) \tag{11.38}$$

where:

$N_B = N_a$ (acceptor concentration)
$N_C = N_d$ (donor concentration) for *npn*-BJTs

- *Effect of diffusion capacitances*: The transition of injected minority carrier charge determines the speed of the transistor. The injected minority carriers from the emitter diffuse through the (1) EB-junction space-charge region, (2) neutral base region, and (3) CB-junction space-charge region. Thus, we consider three diffusion capacitances for forward injection and three for reverse injection.

  Let us consider the capacitance effect due to the injected charge in the EB space-charge layer as shown in Figure 11.17. Let us define Q_E, Q_{BE}, Q_B, and Q_{BC} as the components of the total diffusion charge Q_{DE} in the emitter, EB-junction space-charge layer, neutral base, and CB-junction depletion regions, respectively. If τ_{Fdc} is the total

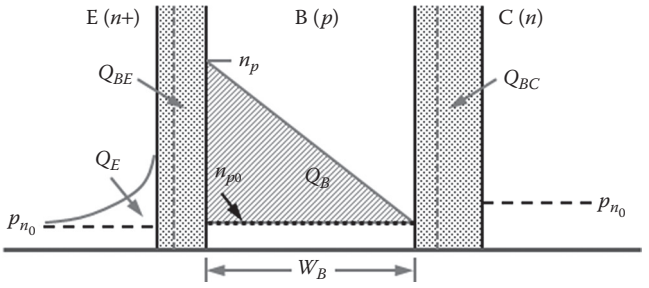

FIGURE 11.17
The components Q_E, Q_{BE}, Q_B, and Q_{BC} of the total diffusion charge Q_{DE} due to the forward injection of carriers at the EB-junction of an *npn*-BJT, resulting in the diffusion capacitance, C_{DE}; n_p is the injected electron concentration at the edge of the EB-depletion region inside the base; p_{n_0} and n_{p0} are the equilibrium minority carrier concentrations in the *n* and *p* regions, respectively; and W_B is the width of the neutral base region.

forward transit time of the carriers to reach from the emitter to collector, then the total minority carrier charge due to forward current I_{CC} is given by

$$Q_{DE} = Q_E + Q_{BE} + Q_B + Q_{BC} = (\tau_E + \tau_{EB} + \tau_B + \tau_{CB})I_{CC} = \tau_{Fdc} I_{CC} \tag{11.39}$$

where:

τ_{Fdc} is the total forward delay time consisting of emitter delay τ_E
EB space charge layer transit time τ_{EB}
base transit time τ_B
CB-space charge layer transit time τ_{CB}

From Equation 11.39, we can write the expression for the diffusion capacitance $C_{DE}(V_{BE})$ due to the applied bias V_{BE}

$$C_{DE}(V_{BE}) = \frac{Q_{DE}}{V_{B'E'}} = \frac{\tau_{Fdc} I_{CC}}{V_{B'E'}} \tag{11.40}$$

The base transit time τ_B is the major contributor of total transistor delay time τ_{Fdc} given in Equation 11.39. Thus, τ_B is the most critical parameter to determine the speed of BJTs. In the absence of built-in electric fields in the base (i.e., constant N_a) with low-level injection, the injected *electron* concentration n_p varies linearly across the base from n_p to $n_{p0} \approx 0$ as shown in Figure 11.17. Therefore, for low-level injection and uniformly doped base region, the total electron charge in the base is simply given by

$$Q_B = \frac{1}{2} q W_B n_p A_E \tag{11.41}$$

where:

A_E = emitter area

n_p is the injected electron concentration at the edge of EB-junction depletion region as shown in Figure 11.17

W_B is the width of the neutral base region

Then the minority carrier transit time across the base is given by

$$\tau_B = \frac{Q_B}{I_{CC}} \tag{11.42}$$

Since the built-in electric field within base is assumed to be negligible, from the Fick's first law of diffusion, we can show that the electron diffusion current (Equation 2.40) is

$$I_{CC} = qA_E D_n \frac{dn_p}{dx} \tag{11.43}$$

where:

D_n is the average electron diffusivity in the *p*-type base region of an *npn*-BJT

Assuming the equilibrium electron concentration, $n_{p0} << n_p$, we can express Equation 11.43 as

$$I_{CC} \cong qA_E D_n \frac{n_p}{W_B} \tag{11.44}$$

Now, substituting for Q_B and I_{CC} from Equations 11.41 and 11.44, respectively, in Equation 11.42, we get the expression for base transit time as

$$\tau_B = \frac{W_B^2}{2D_n} \tag{11.45}$$

To understand the importance of τ_B in determining the speed of BJTs, let us consider a vertical *npn*-BJT with $W_B = 1$ μm and lightly doped base so that $D_n \cong 38$ cm^2 sec^{-1}. Then from Equation 11.45, we find that the value of $\tau_B \cong 132$ psec for a uniformly doped base region. In reality, the base doping is graded, and therefore, an aiding electric field speeds up the carrier transit through the base. As a result, τ_B is further reduced. Also, in order to maintain the charge neutrality under high-level injection, the hole concentration in the base has a gradient similar to the electron gradient. This sets up an electron field, which also speeds up the electron transit through the base. Thus, τ_B is not the dominant frequency limitation in advanced IC BJTs.

Similarly, we can derive the expression for the reverse diffusion capacitance C_{DC} and transit time τ_{Rdc} with reference to Figure 11.18.

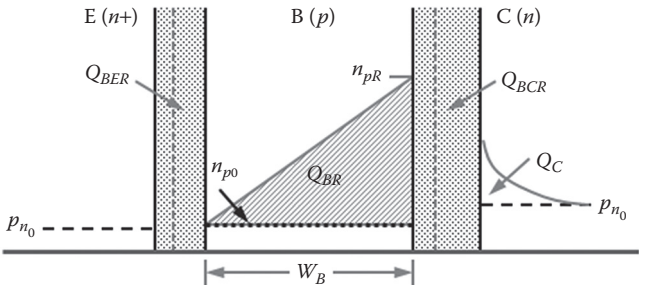

FIGURE 11.18
The components Q_C, Q_{BCR}, Q_{BR}, and Q_{BER} of the total diffusion charge Q_{DC} due to the reverse injection of carriers at the CB-junction of an *npn*-BJT resulting in the diffusion capacitance, C_{DC}; n_{pR} is the injected electron concentration at the edge of the CB-depletion region inside the base; p_{n_0} and n_{p_0} are the equilibrium minority carrier concentrations in the *n* and *p* regions, respectively; and W_B is the width of the neutral base region.

From Figure 11.18, the total minority carrier charge Q_{DC} due to the reverse current I_{EC} is given by

$$Q_{DC} = Q_C + Q_{BCR} + Q_{BR} + Q_{BER} = (\tau_C + \tau_{CB} + \tau_{BR} + \tau_{EB})I_{EC} = \tau_{Rdc} I_{EC} \quad (11.46)$$

where:

Q_C, Q_{BCR}, Q_{BR}, and Q_{BER} are the reverse-injected charge in the collector, CB-depletion, base, and EB-depletion regions, respectively

the total reverse delay time τ_{Rdc} consists of the collector delay τ_C, CB-junction reverse space-charge layer transit time τ_{CB}, reverse base transit time τ_{BR}, and reverse EB-junction space-charge layer transit time τ_{EB}

Therefore, the reverse diffusion capacitance due to CB applied bias V_{BC} is given by

$$C_{DC}(V_{BC}) = \frac{Q_{DC}}{V_{B'C'}} = \frac{\tau_{Rdc} I_{EC}}{V_{B'C'}} \quad (11.47)$$

11.5.2.2 Limitations of Basic Model

The enhanced BJT model includes parasitic elements in BJT structure to improve DC modeling accuracy and offers capability for transient analysis. However, the model is derived on the assumptions that (1) there is no recombination of minority carriers in the EB and CB *pn*-junction space-charge regions; (2) current gain β is independent of I_C; and (3) the neutral base width W_B is independent of applied bias V_{BC}, that is, no space-charge widening and *base-width modulation*. However, experimental data show β-degradation at the low values of EB-junction bias or low values of I_C, and β-roll-off at high

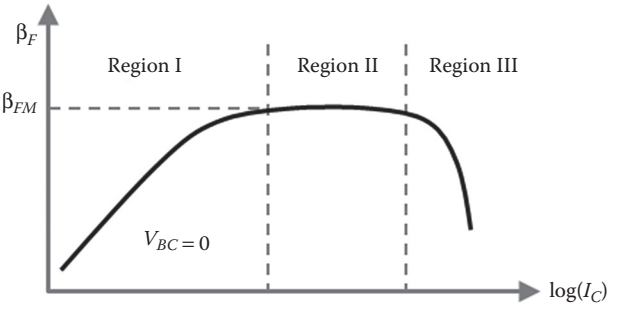

FIGURE 11.19
Forward current gain as a function of collector current of an *npn*-BJT showing three different $\beta - I_C$ regions: region I shows β-degradation in the low current level, region II shows the constant maximum current gain β_{FM}, and region III shows β roll-off at high current level.

current conditions as shown in Figure 11.19. Figure 11.19 shows $\beta_F - I_C$ plot at $V_{BC} = 0$. For the simplicity of discussions, we assume that the ohmic drop due to the parasitic resistances is negligibly small so that $V_{BE} \cong V_{B'E'}$ and $V_{BC} \cong V_{B'C'}$.

In order to understand the underlying physical mechanisms of $\beta_F - I_C$ plot shown in Figure 11.19, let us plot $\ln(I_C, I_B)$ as a function of V_{BE} at $V_{BC} = 0$ as shown in Figure 11.20. Figure 11.20 is often referred to as the *Gummel plot*.

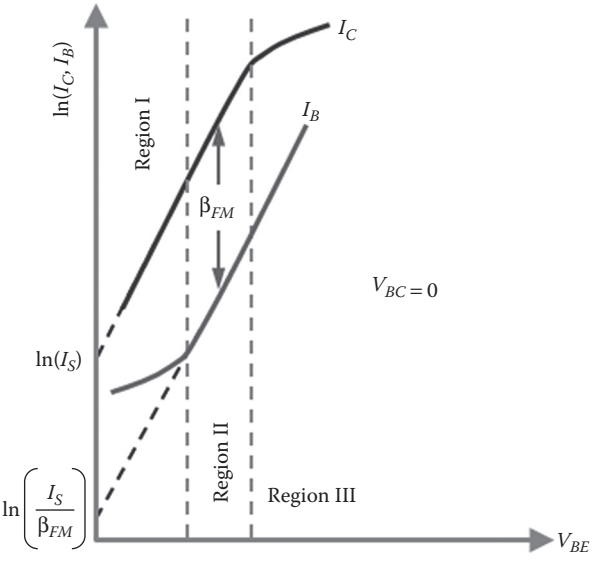

FIGURE 11.20
A typical Gummel plot of an *npn*-BJT: I_C and I_B versus V_{BE} at $V_{BC} = 0$ showing β-degradation at the low current level and β-roll-off at the high collector current level; β_{FM} is the maximum value of current gain.

It is observed from Figure 11.20 that the β-degradation at low current level is due to the increase in the base current, whereas β-roll-off at high current condition is due to the decrease in the collector current. The observed β-degradation at low current level is attributed to the recombination of injected carriers in the space-charge regions whereas β-roll-off at high current condition is due to the high-level injection.

Thus, in order to improve the simulation accuracy, we will develop models for minority carrier recombination in the space-charge regions, base-width modulation, and high-level injection to include in the BJT model described in Figure 11.13. First of all, we will develop models for the minority carrier recombination in the EB and CB *pn*-junction depletion regions and include in the model shown in Figure 11.13. Finally, we will include models for the base-width modulation and high-level injection and present a complete compact BJT model for circuit CAD.

11.5.3 Modeling Carrier Recombination in the Depletion Regions

In Region I of Figure 11.20, the increase in I_B is due to the minority carrier recombination in the EB and CB *pn*-junction depletion regions. For the simplicity of analysis, we assume a vertical *npn*-BJT in the normal active mode of operation and neglect the ohmic-bulk resistors (r_e, r_b, r_c) so that $V_{BE} = V_{B'E'}$ and $V_{BC} = V_{B'C'}$.

Let us consider the effect of the minority carrier recombination in the EB-depletion region only by setting $V_{BC} = 0$. In Region I, the decrease in β can be modeled by additional components of I_B from

- Carrier recombination at the surface, I_B(surface)
- Carrier recombination in the EB space-charge layer, I_B(EB-scl)
- EB surface channels, I_B(channel)

Thus, the overall excess base current can be represented by

$$\Delta I_B(\text{total}) = I_B\left(\text{surface}\right) + I_B\left(\text{EB-scl}\right) + I_B\left(\text{channel}\right) \tag{11.48}$$

In Equation 11.48, ΔI_B can be represented by an additional nonideal EB *pn*-junction in the model shown in Figure 11.13 with diode current given by

$$\Delta I_B = C_2 I_S(0)\left[\exp\left(\frac{V_{BE}}{n_E v_{kT}}\right) - 1\right] \tag{11.49}$$

where:

n_E is the low-current forward emission coefficient (~2)

C_2 models the various components of I_S in the low I_B regime

Here, $I_S(0)$ is the revised reverse saturation current of the transistor. Thus, combining Equations 11.20 and 11.49, the forward diode current can be modeled by

$$I_B = \frac{I_S(0)}{\beta_{FM}}\left[\exp\left(\frac{V_{BE}}{v_{kT}}\right)-1\right]+C_2 I_S(0)\left[\exp\left(\frac{V_{BE}}{n_E v_{kT}}\right)-1\right] \tag{11.50}$$

Similarly, we can model the minority carrier recombination in the CB-depletion region only by another nonideal CB *pn*-junction by setting $V_{BE} = 0$ in the *inverse mode* of BJT operation with $V_{BC} > 0$. Two additional parameters used to model the components of I_B are low-current inverse emission coefficient n_C (~2) and component of I_S in the inverse region C_4. Thus, ΔI_B in the inverse region is through the nonideal CB-diode is given by

$$\Delta I_{BR} = C_4 I_S(0)\left[\exp\left(\frac{V_{BC}}{n_C v_{kT}}\right)-1\right] \tag{11.51}$$

Thus, the general expression for total I_B to model β-degradation in the low I_C region is given by

$$\begin{aligned} I_B = {} & \frac{I_S(0)}{\beta_{FM}}\left[\exp\left(\frac{V_{BE}}{v_{kT}}\right)-1\right]+C_2 I_S(0)\left[\exp\left(\frac{V_{BE}}{n_E v_{kT}}\right)-1\right] \\ & +\frac{I_S(0)}{\beta_{RM}}\left[\exp\left(\frac{V_{BC}}{v_{kT}}\right)-1\right]+C_4 I_S(0)\left[\exp\left(\frac{V_{BC}}{n_C v_{kT}}\right)-1\right] \end{aligned} \tag{11.52}$$

Note that in Equation 11.52, we have used maximum current gain (β_{FM}, β_{RM}) *to model the EB and CB* pn*-junctions and included the excess* I_B *to account for the* β*-degradation in the low current level.* Then the corresponding equivalent circuit for enhanced nonlinear hybrid *npn*-BJT model predicting β versus I_C at low current level can be represented by Figure 11.21.

Note that the series resistances (r_e, r_b, r_c) *do not effect theoretical analysis and model equations. However, one should replace measured* V_{BE} *and* V_{BC} *with the internal voltages to account for the ohmic drops in the model equations.*

In order to develop a complete compact BJT model for circuit CAD, we now include the effect of base-width modulation referred to as the *early effect* [8] and high-level injection to model β roll-off in the high current level shown in Figure 11.19 in the core model shown in Figure 11.21. In this effort, we will closely follow the *unified charge-control* model developed by Gummel and Poon [6].

11.5.4 Modeling Base-Width Modulation and High-Level Injection

The base-width modulation describes the change in the quasi-neutral base-region W_B due to the change in the reverse bias V_{BC} in the *normal active* mode

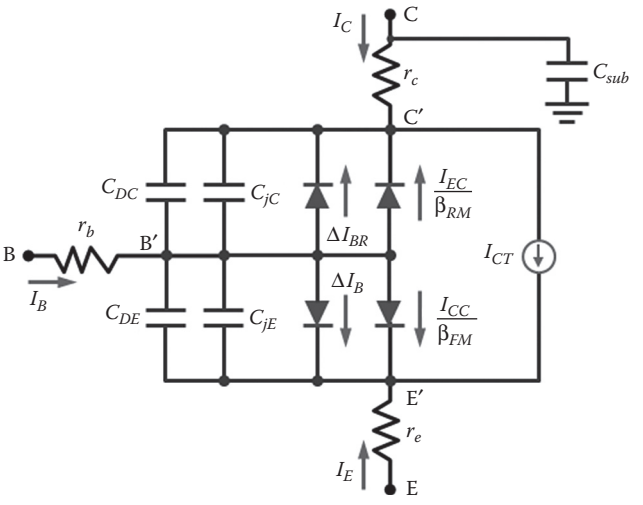

FIGURE 11.21
The equivalent circuit of the enhanced vertical *npn*-BJT model to model β-degradation in the low current level using two nonideal diodes to account for increased base current due to recombination in the depletion regions. $\Delta I_B = C_2 I_S(0)\left[\exp\left(V_{BE}/n_E v_{kT}\right) - 1\right]$ is the excess forward base current due to the nonideal EB diodes and $\Delta I_{BR} = C_4 I_S(0)\left[\exp\left(V_{BC}/n_C v_{kT}\right) - 1\right]$ is the excess reverse base current due to the nonideal CB diodes.

(or V_{BE} in the *inverse* mode). In the normal active mode of BJT operation, EB-junction is forward biased and CB-junction is reverse biased. As a result, the depletion width $X_d = f(V_{BC})$ and the neutral base width W_B as shown in Figure 11.22 change significantly with V_{BC}. This base-width modulation is originally reported by J. Early in 1952 and is called the *early effect* [8]. The concept is now used in MOSFET device characterization as discussed in Chapters 4 and 5. The early effect changes $I_C - V_{CE}$ characteristics of BJTs

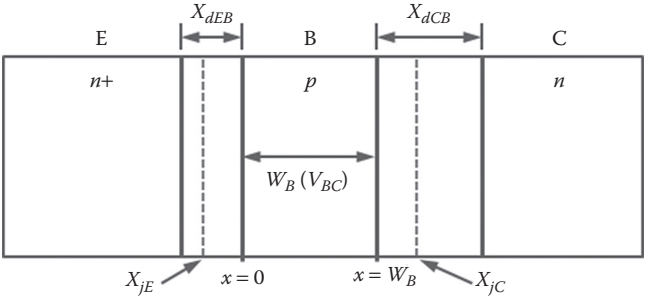

FIGURE 11.22
An idea *npn*-BJT device structure for modeling the early effect: X_{dEB} and x_{dCB} are the depletion widths of EB and CB *pn*-junction space-charge regions, respectively; $W(V_{BC})$ is the bias-dependent base width; $x = 0$ is the origin of *x*-axis at the edge of EB-junction depletion inside the base; and $x = W_B$ is at the edge of CB-junction depletion region inside the base.

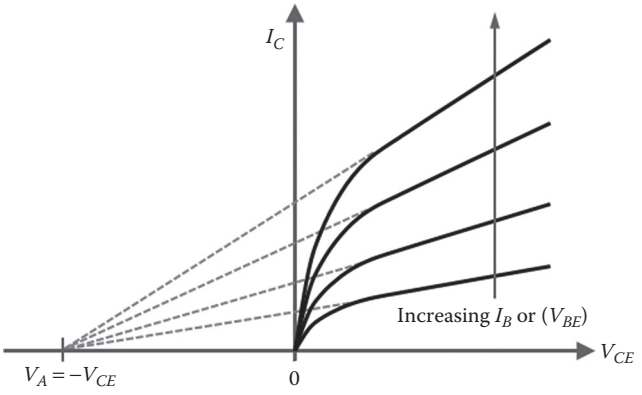

FIGURE 11.23
I_C versus V_{CE} characteristics of a typical *npn*-BJT for different values of I_B or V_{BE}; the increase in I_C is caused by base-width modulation at higher V_{BC}; V_A is defined at the intercept of $I_C - V_{CE}$ curve interpolated to $I_C = 0$.

significantly and, therefore, must be modeled for accurate simulation of BJTs in circuit CAD.

As the reverse bias V_{BC} across the BC-junction X_{jC} increases, BC-junction depletion-layer width X_{dCB} increases, resulting in a decrease in W_B. Due to the decrease in W_B, the injected minority carrier electron concentration gradient (dn/dx) increases. Then from Fick's first law of diffusion, I_C increases with V_{CE} as shown in Figure 11.23. The base-width modulation is modeled by two parameters called the forward early voltage (V_{AF}) and reverse early voltage (V_{AR}). Due to the early effect, the BJT device parameters I_S, β_F, and τ_F strongly depend on V_{BC} and V_A [5].

In order to derive the unified SGP charge control model [6] for base-width modulation and high-level injection, let us make the following simplifying assumptions:

Assumption 1: one-dimensional current equations hold.

Assumption 2: *npn*-BJT with EB-junction is forward biased and CB-junction is reverse biased.

Assumption 3: depletion approximation holds, that is, no mobile charge inside the depletion region.

Assumption 4: BJT gain is high, that is, $I_B \cong 0$.

Assumption 5: neglect ohmic-bulk resistors (r_e, r_b, r_c); that is, $V_{BE} = V_{B'E'}$ and $V_{BC} = V_{B'C'}$.

With the above simplifying assumptions, let us consider the 2D cross section of an *npn*-BJT shown in Figure 11.24.

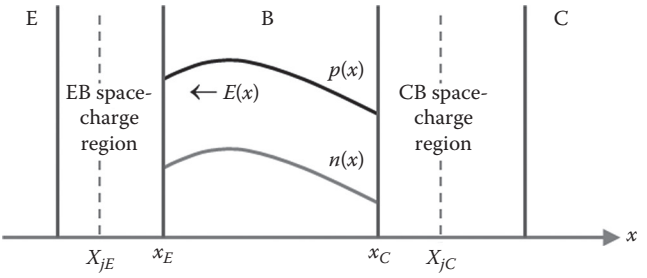

FIGURE 11.24
2D cross section of an ideal *npn*-BJT showing the *pn*-junctions and depletion regions: $p(x)$ and $n(x)$ are the majority and minority carrier concentrations, respectively, at any point x in the neutral base region; x_E and x_C are the position of the EB and CB depletion edges inside the base, respectively; and $E(x)$ is the built-in electric field from collector to emitter due to the nonuniform p-type base doping profile.

Using assumption 1, we can use 1D expression for the electron and hole current densities (Equations 2.76 and 2.77) as

$$\begin{aligned} J_n &= q\mu_n n(x)E(x) + qD_n \frac{dn}{dx} \quad \text{(electrons)} \\ J_p &= q\mu_p p(x)E(x) - qD_p \frac{dp}{dx} \quad \text{(holes)} \end{aligned} \tag{11.53}$$

Now from assumption 4, for a high-gain *npn*-BJT, $I_B \cong 0$, that is, the hole current $\cong 0$; then from the hole current expression J_p in Equation 11.53, we get

$$0 = q\mu_p p(x)E(x) - qD_p \frac{dp}{dx} \tag{11.54}$$

After simplification of Equation 11.54 and using Equation 2.42, we can show that the built-in electric field $E(x)$ due to nonuniform base doping of *npn*-BJTs is given by (Equation 2.46)

$$E(x) = \frac{D_p}{\mu_p}\frac{1}{p(x)}\frac{dp}{dx} = v_{kT}\frac{1}{p(x)}\frac{dp}{dx} \tag{11.55}$$

The direction of the electric field $E(x)$ in Equation 11.55 aids the electron flow from the emitter to collector and retards the electron flow from the collector to emitter. Now, the flow of electrons from the emitter to collector is given by the electron current expression J_n in Equation 11.53. Then, substituting for $E(x)$ from Equation 11.55 to Equation 11.53 we get

$$J_n = q\mu_n n(x)\left[v_{kT}\frac{1}{p(x)}\frac{dp(x)}{dx}\right] + qD_n\frac{dn}{dx} \tag{11.56}$$

Using $\mu_n v_{kT} = D_n$ from Einstein's relation [Equation 2.42], we can express Equation 11.56 after simplification as

$$J_n = \frac{qD_n}{p(x)} \frac{d}{dx}\big(n(x)p(x)\big) \tag{11.57}$$

We integrate Equation 11.57 over the neutral base width W_B from $x = x_E$ to $x = x_C$ as shown in Figure 11.24 to get

$$\int_{x_E}^{x_C} J_n p(x)dx = q\int_{x_E}^{x_C} D_n d\big[n(x)p(x)\big] \tag{11.58}$$

Since the same collector current density J_n is flowing through the BJT, J_n is a constant. Then assuming D_n is a constant, we can show from Equation 11.58

$$J_n = \frac{qD_n\big[pn(x_C) - pn(x_E)\big]}{\int_{x_E}^{x_C} p(x)dx} \tag{11.59}$$

From Equation 11.59, we find that the electron current, that is, collector current density, depends on *pn*-products at the edges of the depletion regions of EB and CB *pn*-junctions inside the base and the integrated base doping in the denominator of Equation 11.59. Again, from *pn*-junction analysis (Equation 2.114), we can show that the *pn*-products at the edges of the collector and emitter depletion regions are

$$\begin{aligned} pn(x_C) &= n_i^2 \exp\left(\frac{V_{BC}}{v_{kT}}\right) \\ pn(x_E) &= n_i^2 \exp\left(\frac{V_{BE}}{v_{kT}}\right) \end{aligned} \tag{11.60}$$

Now, substituting for *pn*-products from Equation 11.60 to Equation 11.59, we can show

$$J_n = \frac{qD_n n_i^2\big[\exp(V_{BC}/v_{kT}) - \exp(V_{BE}/v_{kT})\big]}{\int_{x_E}^{x_C} p(x)dx} \tag{11.61}$$

If A_E is cross-sectional area of the emitter, then from Equation 11.61 we can show

$$\begin{aligned} I_n &= \frac{qA_E D_n n_i^2 \left[\exp\left(V_{BC}/v_{kT}\right) - \exp\left(V_{BE}/v_{kT}\right)\right]}{\int_{x_E}^{x_C} p(x)dx} \\ &= -\frac{qA_E D_n n_i^2}{\int_{x_E}^{x_C} p(x)dx}\left\{\left[\exp\left(\frac{V_{BE}}{v_{kT}}\right)-1\right]-\left[\exp\left(\frac{V_{BC}}{v_{kT}}\right)-1\right]\right\} \end{aligned} \tag{11.62}$$

where:

I_n is the total DC current from the emitter to base in the positive x-direction due to the minority carrier electrons

Since at *low-level injection* $p(x) \cong N_a(x)$, in the neutral base region, $x_E \le x \le x_C$ as shown in Figure 11.24; then by replacing the injected $p(x)$ with the majority carrier concentration, we can write Equation 11.62 as

$$I_{n(low\text{-}level)} = -\frac{qA_E D_n n_i^2}{\int_{x_E}^{x_C} N_a(x)dx}\left\{\left[\exp\left(\frac{V_{BE}}{v_{kT}}\right)-1\right]-\left[\exp\left(\frac{V_{BC}}{v_{kT}}\right)-1\right]\right\} \tag{11.63}$$

We have shown that the current source for the basic BJT model (Equation 11.19) is given by

$$I_{CT} = \left(I_{CC} - I_{EC}\right) = I_S\left\{\left[\exp\left(\frac{V_{BE}}{v_{kT}}\right)-1\right]-\left[\exp\left(\frac{V_{BC}}{v_{kT}}\right)-1\right]\right\} \tag{11.64}$$

Therefore, comparing Equations 11.63 and 11.64, we can write for low-level injection

$$I_{CT(low\text{-}level)} = I_{SS}\left\{\left[\exp\left(\frac{V_{BE}}{v_{kT}}\right)-1\right]-\left[\exp\left(\frac{V_{BC}}{v_{kT}}\right)-1\right]\right\} \tag{11.65}$$

where:

I_{SS} is the saturation leakage current at $V_{BE} = V_{BC} = 0$

and is given by

$$I_{SS} = -\frac{qA_E D_n n_i^2}{\int_{x_{E0}}^{x_{C0}} N_a(x)dx} \tag{11.66}$$

where:

X_{E0} and X_{C0} are the locations inside the neutral base region at the edge of the EB- and CB-junction depletion regions, respectively without the applied bias

Thus, I_{SS} defined in Equation 11.66 is a bias-independent fundamental constant. Since negative sign indicates the direction of collector current flowing out of the device terminal, we have omitted the negative sign in the above Equation 11.65. Now, Equation 11.63 can be expressed as

$$\begin{aligned} I_{CT} &= \frac{qA_E D_n n_i^2}{\int_{x_E}^{x_C} p(x)dx} \cdot \left(\frac{qA_E \int_{x_{E0}}^{x_{C0}} N_a(x)dx}{qA_E \int_{x_{E0}}^{x_{C0}} N_a(x)dx} \right) \times \\ &\quad \left\{ \left[\exp\left(\frac{V_{BE}}{v_{kT}} \right) - 1 \right] - \left[\exp\left(\frac{V_{BC}}{v_{kT}} \right) - 1 \right] \right\} \\ &= \frac{qA_E D_n n_i^2}{\int_{x_{E0}}^{x_{C0}} N_a(x)dx} \cdot \left(\frac{qA_E \int_{x_{E0}}^{x_{C0}} N_a(x)dx}{qA_E \int_{x_E}^{x_C} p(x)dx} \right) \times \\ &\quad \left\{ \left[\exp\left(\frac{V_{BE}}{v_{kT}} \right) - 1 \right] - \left[\exp\left(\frac{V_{BC}}{v_{kT}} \right) - 1 \right] \right\} \end{aligned} \tag{11.67}$$

If we define Q_B and Q_{B0} as the neutral base charges with and without the applied biases, respectively, then we can show

$$\begin{aligned} Q_{B0} &= qA_E \int_{x_{E0}}^{x_{C0}} N_a(x)dx \\ Q_B &= qA_E \int_{x_{E(V_{BE})}}^{x_C(V_{BC})} N_a(x)dx \end{aligned} \tag{11.68}$$

Now, using Equation 11.68 in Equation 11.67, we can show that the expression for current source for an *npn*-BJT is given by

$$\begin{aligned} I_{CT} &= I_{SS} \frac{Q_{B0}}{Q_B} \left\{ \left[\exp\left(\frac{V_{BE}}{v_{kT}} \right) - 1 \right] - \left[\exp\left(\frac{V_{BC}}{v_{kT}} \right) - 1 \right] \right\} \\ &= \frac{I_{SS}}{q_b} \left\{ \left[\exp\left(\frac{V_{BE}}{v_{kT}} \right) - 1 \right] - \left[\exp\left(\frac{V_{BC}}{v_{kT}} \right) - 1 \right] \right\} \end{aligned} \tag{11.69}$$

In Equation 11.69, q_b is the normalized base charge and is defined as

$$q_b = \frac{Q_B}{Q_{B0}} \tag{11.70}$$

Equation 11.69 is the generalized expression for current source at all injection levels, where I_{SS} is a fundamental constant @ $V_{BE} = V_{BC} = 0$ and is given by Equation 11.66. The normalized majority carrier charge q_b in the neutral base region accurately models the base-width modulation. In the next section, we will express q_b in terms of bias-dependent measurable model parameters.

11.5.4.1 Components of Injected Base Charge

In order to evaluate q_b, we first determine the components of Q_B. For the simplicity of Q_B analysis, we assume that

- *npn*-BJT is in *saturation*, that is, $V_{BE} > 0$ and $V_{BC} > 0$, then
  - Minority carriers are injected into the base both from the *emitter* and from the *collector*
  - From the charge neutrality, the total increase in the majority carriers in the *base* = total increase in the minority carrier concentration
- *Superposition* of carriers in different regions holds, that is
  - Total *excess* majority carrier density = sum of the *excess* majority carrier density due to each junction separately
  - Excess majority carrier concentration in the base = excess carriers due to the forward voltage ($V_{BE} + V_{BC}$)
  - Depletion approximation holds

With the above assumptions, we define

- $p_F(x)$ as the majority carrier concentration at any point x in the base at $V_{BC} = 0$
- $p_R(x)$ as the majority carrier concentration at any point x in the base at $V_{BE} = 0$
- $N_a(x)$ as the base doping concentration at any point x

Then the excess majority carrier concentration in the base region is shown in Figure 11.25 and is given by

$$p'(x) = \left[p_F(x) - N_a(x)\right] + \left[p_R(x) - N_a(x)\right] \tag{11.71}$$

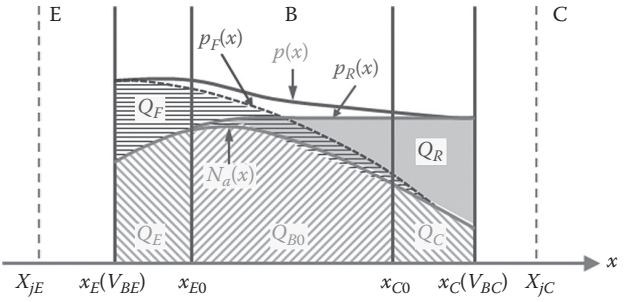

FIGURE 11.25
The components of base charge in an *npn*-BJT in saturation: Q_{B0} is the base charge in the neutral base region without applied biases; Q_E and Q_C are the increase in the base charge due to the EB and CB forward biases, respectively; Q_F and Q_R are the excess charge due to the high-level injection from the emitter and collector, respectively, to the base; $p_F(x)$ and $p_R(x)$ are the excess majority carrier concentration in the base region from emitter and collector, respectively

From Equation 11.68, the total majority carrier charge in the base consists of *equilibrium charge* due to N_a and *excess components* due to $p'(x)$ and is given by

$$Q_B = qA_E \int_{x_{E(V_{BE})}}^{x_C(V_{BC})} p(x)dx = \int_{x_{E(V_{BE})}}^{x_C(V_{BC})} qA_E N_a(x)dx + \int_{x_{E(V_{BE})}}^{x_C(V_{BC})} qA_E p'(x)(x)dx \tag{11.72}$$

The equilibrium base charge includes three components: Q_E due to the decrease in the depletion region by the forward-biased EB-junction space charge region, Q_{B0} due to the neutral base charge, and Q_C due to the decrease in the depletion charge by the forward-biased BC-junction depletion region as shown in Figure 11.25. Therefore, the total equilibrium component of the base charge under the saturation condition is given by

$$\begin{aligned}\int_{x_{E(V_{BE})}}^{x_C(V_{BC})} qA_E N_a(x)dx &= Q_E + Q_{B0} + Q_C \\ &= \int_{x_{E(V_{BE})}}^{x_{E0}} qA_E N_a(x)dx + \int_{x_{E0}}^{x_{C0}} qA_E N_a(x)dx + \int_{x_{C0}}^{x_C(V_{BC})} qA_E N_a(x)dx\end{aligned} \tag{11.73}$$

Therefore, from Equations 11.72 and 11.73, the total base charge due to EB and CB-junction forward biases is given by

$$\begin{aligned}Q_B = &\int_{x_{E(V_{BE})}}^{x_{E0}} qA_E N_a(x)dx + \int_{x_{E0}}^{x_{C0}} qA_E N_a(x)dx \\ &+ \int_{x_{C0}}^{x_C(V_{BC})} qA_E N_a(x)dx + \int_{x_{E(V_{BE})}}^{x_C(V_{BC})} qA_E p'(x)dx\end{aligned} \tag{11.74}$$

From Figure 11.25, we find that the excess forward charge is due to the forward injection carrier profile $[p_F(x) - N_a(x)]$ and reverse injection carrier density profile $[p_R(x) - N_a(x)]$. Therefore, the excess carrier density is given by

$$\begin{aligned}\int_{x_{E(V_{BE})}}^{x_C(V_{BC})} qA_E p'(x)dx &= \int_{x_{E(V_{BE})}}^{x_C(V_{BC})} qA_E\left[p_F(x) - N_a(x)\right]dx \\ &\quad + \int_{x_{E(V_{BE})}}^{x_C(V_{BC})} qA_E\left[p_R(x) - N_a(x)\right]dx \\ &= Q_F + Q_R\end{aligned} \tag{11.75}$$

Therefore, the total base charge due to the applied EB- and CB-junction biases is given by

$$Q_B = Q_E + Q_{B0} + Q_C + Q_F + Q_R \tag{11.76}$$

where:

Q_{B0} is the charge in the neutral base region at $V_{BE} = 0 = V_{BC}$
Q_E is the increase in Q_B under V_{BE} and is only a mathematical entity
Q_C is the increase in Q_B under V_{BC} and is only a mathematical entity
Q_F is the excess majority charge in the forward biased-device with $V_{BC} = 0$. It is only a mathematical entity and important under high level injection
Q_R is the excess majority charge in the forward biased-device with $V_{BE} = 0$. It is only a mathematical entity and important under *high-level injection*

It is clear from Figure 11.25 that $p_F(x) > N_a(x)$ and $p_R(x) > N_a(x)$, that is, Q_F and Q_R represent high-level injection. Then from Equation 11.76, we get the normalized components of base charge as

$$\frac{Q_B}{Q_{B0}} = \frac{Q_E}{Q_{B0}} + \frac{Q_{B0}}{Q_{B0}} + \frac{Q_C}{Q_{B0}} + \frac{Q_F}{Q_{B0}} + \frac{Q_R}{Q_{B0}} \tag{11.77}$$

After simplification, we can show for the normalized base charge from Equation 11.77

$$q_b = 1 + q_e + q_c + q_f + q_r \tag{11.78}$$

where:

$q_e = Q_E/Q_{B0}$, $q_c = Q_C/Q_{B0}$, $q_f = Q_F/Q_{B0}$, and $q_e = Q_R/Q_{B0}$ are the respective normalized components of base charge

In order to develop BJT compact model, each component of the normalized base charge is expressed in terms of measurable device model parameters. Next, we will evaluate each component of q_b given in Equation 11.78.

Evaluation of q_e: We defined Q_E as the increase in the majority carrier charge due to forward bias V_{BE}. Therefore, we can express

$$Q_E = \int_0^{V_{BE}} C_{jE}(V)dV \tag{11.79}$$

and,

$$q_e = \frac{1}{Q_{B0}} \int_0^{V_{BE}} C_{jE}(V)dV \tag{11.80}$$

For the simplicity of modeling, we consider an average value $\overline{C}_{jE}$ over the operating range of V_{BE}. Then from Equation 11.80, we get

$$q_e = \frac{\overline{C}_{jE}}{Q_{B0}} V_{BE} \equiv \frac{V_{BE}}{V_{AR}} \tag{11.81}$$

where:

V_{AR} is a model parameter that defines the effect of base-width modulation due to V_{BE} and the parameter V_{AR} is called the inverse early voltage

From Equation 11.81, we get

$$V_{AR} = \frac{Q_{B0}}{\overline{C}_{jE}} \tag{11.82}$$

However, for accurate modeling of q_e, C_{jE} must be integrated over the operating bias range so that

$$V_{AR} = \frac{Q_{B0}}{(1/V_{BE}) \int_0^{V_{BE}} C_{jE}(V)dV} \tag{11.83}$$

In Equation 11.81, V_{AR} models the base-width modulation due to the variation of BE-junction depletion layer under V_{BE} and is the inverse of the forward early voltage due to V_{BC} under the normal mode of BJT operation.

In Equation 11.82, a constant V_{AR} implies that C_{jE} is a constant, independent of V_{BE}. We observe from Figure 11.25 that $Q_E << Q_{B0}$, resulting in $q_e << 1$. Thus, q_e is not a dominant component of q_b. Therefore, using a constant C_{jE} to calculate q_e from Equation 11.81 is justified. However, a constant V_{AR} may cause a large error in q_e estimation, especially at $V_{BE} > 0$. The error in Equation 11.81 due to q_e for $V_{BE} > 0$ can be eliminated by integrating C_{jE} over the operating bias range and extracting V_{AR} from the slope of $\ln(I_C)$ versus V_{BE}/v_{kT} plot.

Now, in order to determine the effect of q_e on BJT device performance, we set: $q_c = q_r = q_f = 0$; then from Equation 11.78, we have $q_b = 1 + q_e$. Now, substituting for $q_b = (1 + q_e)$ in Equation 11.69, we get

$$I_C = I_{CT} = \frac{I_{SS}}{(1+q_e)}\left[\exp\left(\frac{V_{BE}}{v_{kT}}\right)-1\right] \tag{11.84}$$

We can calculate the slope of I_C versus V_{BE} plot by differentiating Equation 11.84 as

$$\frac{dI_C}{dV_{BE}} = \frac{I_C}{v_{kT}}\left[1 - v_{kT}\frac{C_{jE}(V_{BE})}{q(1+q_e)Q_{B0}}\right]$$

or,

$$v_{kT}\frac{1}{I_C}\frac{dI_C}{dV_{BE}} = \frac{d(\ln(I_C))}{d(V_{BE}/v_{kT})} = \left[1 - v_{kT}\frac{C_{jE}(V_{BE})}{q(1+q_e)Q_{B0}}\right] \tag{11.85}$$

The left-hand side of Equation 11.85 is the slope of $\ln(I_C)$ versus V_{BE}/v_{kT} plot and is given by

$$\frac{1}{n_E} = v_{kT}\frac{1}{I_C}\frac{dI_C}{dV_{BE}}\bigg|_{V_{BC}=0} = \left[1 - v_{kT}\frac{C_{jE}(V_{BE})}{q(1+q_e)Q_{B0}}\right] \tag{11.86}$$

Thus,

$$n_E = \frac{1}{1 - v_{kT}\left[C_{jE}(V_{BE})/q(1+q_e)Q_{B0}\right]} \tag{11.87}$$

Considering a constant average $\overline{C}_{jE} = Q_{B0}/V_{AR}$ from Equation 11.82, and $q_e = V_{BE}/V_{AR}$ from Equation 11.81, we can express Equation 11.87 as

$$n_E \cong \frac{1}{1-\left[v_{kT}/(V_{AR}+V_{BE})\right]} \tag{11.88}$$

The slope n_E is called the forward emission coefficient and is obtained from the $I_C - V_{BE}$ characteristics of BJTs at $V_{BC} = 0$. Since v_{kT}, V_{AR}, and V_{BE} are finite positive numbers, it is clear from Equation 11.88 that $n_E > 1$.

Evaluation of q_c: The parameter q_c models the base-width modulation due to the applied CB-junction voltage V_{BC} at the low current level during the

forward active mode of a BJT operation and describes the forward early effect. Using the same procedure used for q_e, we can show

$$q_c = \frac{1}{Q_{B0}} \int_0^{V_{BC}} C_{jC}(V)dV \tag{11.89}$$

Again, considering a constant value of $\overline{C}_{jC}$ as the average value of BC-junction capacitance over the operating range of V_{BC}, we get from Equation 11.89

$$q_c = \frac{\overline{C}_{jC}}{Q_{B0}} V_{BC} \equiv \frac{V_{BC}}{V_{AF}} \tag{11.90}$$

where:

V_{AF} is a model parameter that defines the effect of base-width modulation when BJTs operate in the forward active mode and the parameter V_{AF} is called the forward early voltage

Thus, from Equation 11.90, V_{AF} is defined as

$$V_{AF} = \frac{Q_{B0}}{\overline{C}_{jC}} \tag{11.91}$$

However, the accurate modeling of q_c for $V_{BC} > 0$ is achieved by integrating C_{jC} over the operating bias range so that

$$V_{AF} = \frac{Q_{B0}}{\left(1/V_{BC}\right)\int_0^{V_{BC}} C_{jC}(V)dV} \tag{11.92}$$

The parameter V_{AF} models the base-width modulation due to the variation in the CB-junction depletion layer with applied bias V_{BC}. In Equation 11.91, a constant V_{AF} implies that C_{jC} is a constant independent of V_{BC}. This constant C_{jC} is justified in the normal active model of BJT operation when CB-junction is reverse biased; that is, $V_{CB} < 1$. However, using a constant V_{AF} may cause a large error in estimating q_c, when CB-junction is forward biased; that is, the device is in the inverse region or saturation region. In these regions, a more accurate expression for q_c is required for accurate modeling of early voltage.

The effect of q_c on BJT device performance in the normal active region of operation is the finite output conductance g_o. In order to determine the effect of g_o accurately, we set $q_e = q_r = q_f = 0$, so that $q_b = 1 + q_c$. Then neglecting

the bulk-ohmic resistances, we get from Equation 11.69 in the normal active region, we have

$$\begin{aligned} I_C \equiv I_{CT} &= \frac{I_{SS}}{(1+q_c)}\left[\exp\left(\frac{V_{BE}}{v_{kT}}\right)-1\right] \\ &= \frac{I_{SS}}{1+(V_{BC}/V_{AF})}\left[\exp\left(\frac{V_{BE}}{v_{kT}}\right)-1\right] \end{aligned} \tag{11.93}$$

From Equation 11.93, we can show

$$g_o = \left.\frac{dI_C}{dV_{CE}}\right|_{V_{BE}=\text{constant}} \cong \frac{I_C(0)}{V_{AF}} \tag{11.94}$$

where:

$I_C(0)$ is the collector current at $V_{CE} = 0$

Evaluation of q_f: The parameter q_f can be considered as the normalized excess carrier density in the base with EB-junction voltage V_{BE} only and models the high-level injection. From the charge neutrality condition, *total excess majority carriers = total excess minority carriers*. Therefore, for an *npn*-BJT in the normal active mode of operation with $|V_{BE}| > 0$ and $V_{BC} = 0$

$$Q_F = \int_{x_E}^{x_C} qA\left[p_F(x) - N_a(x)\right]dx = \int_{x_E}^{x_C} qA\left[n_F(x) - \frac{n_i^2}{N_a(x)}\right]dx \tag{11.95}$$

We have shown in Equation 11.42 that the minority carrier forward base transit time τ_B of a BJT and the base charge Q_B are given by $Q_B = \tau_B I_{CC}$. Therefore, from Equation 11.95, the forward base transit time can be expressed as

$$Q_F = \tau_{BF} I_{CC} \tag{11.96}$$

where:

$I_{CC} = I_{CT}$ given by Equation 11.69 at $V_{BC} = 0$

τ_{BF} is the forward base transit time

Therefore, the normalized forward injection charge is given by

$$q_f = \frac{Q_F}{Q_{B0}} = \frac{\tau_{BF} I_{CC}}{Q_{B0}} = \frac{\tau_{BF}}{Q_{B0}}\frac{I_{SS}}{q_b}\left[\exp\left(\frac{V_{BE}}{v_{kT}}\right)-1\right] \tag{11.97}$$

Evaluation of q_r: Similar to q_f, q_r can be considered as the normalized excess carrier density in the base due to CB-junction voltage V_{BC} only and models the high-level injection. Again, from the charge neutrality condition, *total*

excess majority carriers = total excess minority carriers. Therefore, for an *npn*-BJT with $|V_{BC}| > 0$; $V_{BE} = 0$, we can show

$$Q_R = \int_{x_E}^{x_C} qA\left[p_R(x) - N_a(x)\right]dx = \int_{x_E}^{x_C} qA\left[n_R(x) - \frac{n_i^2}{N_a(x)}\right]dx \tag{11.98}$$

Again, from Equation 11.47, we can show that the reverse base transit time for BJTs is given by

$$Q_R = \tau_{BR} I_{EC} \tag{11.99}$$

Therefore, the normalized reverse injection charge is given by

$$q_r = \frac{Q_R}{Q_{B0}} = \frac{\tau_{BR} I_{EC}}{Q_{B0}} = \frac{\tau_{BR}}{Q_{B0}} \frac{I_{SS}}{q_b}\left[\exp\left(\frac{V_{BC}}{v_{kT}}\right) - 1\right] \tag{11.100}$$

Equations 11.81, 11.90, 11.97, and 11.100 represent the components of the normalized base charge q_e, q_c, q_f, and q_r, respectively, in terms of measurable device parameters. We will substitute these components of base charges in Equation 11.78 to solve for q_b in the following section.

Evaluation of q_b: Substituting for q_e, q_c, q_f, and q_r from Equations 11.81, 11.90, 11.97, and 11.100, respectively, in Equation 11.78 we can show the expression for total normalized charge as

$$\begin{aligned} q_b &= 1 + \frac{V_{BE}}{V_{AR}} + \frac{V_{BC}}{V_{AF}} + \frac{\tau_f}{Q_{B0}} \frac{I_{SS}}{q_b}\left[\exp\left(\frac{V_{BE}}{v_{kT}}\right) - 1\right] + \frac{\tau_r}{Q_{B0}} \frac{I_{SS}}{q_b}\left[\exp\left(\frac{V_{BC}}{v_{kT}}\right) - 1\right] \\ &= \left(1 + \frac{V_{BE}}{V_{AR}} + \frac{V_{BC}}{V_{AF}}\right) \\ &\quad + \frac{1}{q_b}\left\{\frac{\tau_f}{Q_{B0}} I_{SS}\left[\exp\left(\frac{V_{BE}}{v_{kT}}\right) - 1\right] + \frac{\tau_r}{Q_{B0}} I_{SS}\left[\exp\left(\frac{V_{BC}}{v_{kT}}\right) - 1\right]\right\} \\ &= q_1 + \frac{q_2}{q_b} \end{aligned} \tag{11.101}$$

where we defined

$$\begin{aligned} q_1 &= 1 + \frac{V_{BE}}{V_{AR}} + \frac{V_{BC}}{V_{AF}} \\ q_2 &= \frac{\tau_f I_{ss}\left[\exp\left(V_{BE}/v_{kT}\right) - 1\right] + \tau_r I_{SS}\left[\exp\left(V_{BC}/v_{kT}\right) - 1\right]}{Q_{B0}} \end{aligned} \tag{11.102}$$

In Equations 11.101 and 11.102, τ_f is the effective forward base transit time including the mobile charge in the depletion region (without depletion approximation) and τ_r is the effective reverse base transit time including the mobile charge in the depletion region (without depletion approximation).

In Equation 11.101, q_1 models the base-width modulation and q_2 models the high-level injection. From Equation 11.101, we can show

$$q_b^2 - q_1 q_b - q_2 = 0 \tag{11.103}$$

Equation 11.103 is a quadratic equation in q_b whose solution is given by

$$q_b = \frac{q_1}{2} \pm \frac{1}{2}\sqrt{q_1^2 + 4q_2} \tag{11.104}$$

From Equation 11.78, we know $q_b > 0$; therefore, considering the positive solution only, we get from Equation 11.104

$$q_b = \frac{q_1}{2} + \sqrt{\left(\frac{q_1}{2}\right)^2 + q_2} \tag{11.105}$$

Equation 11.105 offers a solution for I_C and defines the injection level. Let us consider the following cases:

$$\text{Case 1: } q_2 << \left(\frac{q_1}{2}\right)^2 \tag{11.106}$$

Under this condition, we get from Equation 105, $q_b \cong q_1$. Then, setting $q_f = q_r = 0$, this condition represents the *low-level injection* and base-width modulation (q_1 in Equation 11.102)

$$\text{Case 2: } q_2 >> \left(\frac{q_1}{2}\right)^2 \tag{11.107}$$

Under this condition, we get from Equation 11.105, $q_b \cong \sqrt{q_2}$, and therefore represents the *high-level injection* in BJTs.

For the simplicity of modeling, we assume $V_{BC} = 0$ (i.e., $q_r = 0$). Then considering q_2 from Equation 11.102, we get from Equation 11.107 the expression for high-level injection in the forward active mode of *npn*-BJT operation as

$$q_b = \sqrt{q_2} \cong \sqrt{\frac{\tau_f I_{ss}}{Q_{B0}}\left[\exp\left(\frac{V_{BE}}{v_{kT}}\right)\right]} = \sqrt{\frac{\tau_f I_{ss}}{Q_{B0}}}\left[\exp\left(\frac{V_{BE}}{2v_{kT}}\right)\right] \tag{11.108}$$

Then substituting for q_b in Equation 11.69, we get for high-level injection at $V_{BC} = 0$ and $V_{BE} >> v_{kT}$

$$I_{C(high-level)} = I_{CT} \cong \frac{I_{SS}\left[\exp\left(V_{BE}/v_{kT}\right)-1\right]}{\sqrt{\tau_f I_{SS}/Q_{B0}}\exp\left(V_{BE}/2v_{kT}\right)} \cong \sqrt{\frac{Q_{B0}I_{SS}}{\tau_f}}\exp\left(\frac{V_{BE}}{2v_{kT}}\right) \quad (11.109)$$

Again, for *low-level injection*, if we assume $q_e = q_c = 0$, then from Equation 11.78 $q_b = 1$. Then from Equation 11.69, we get for low-level injection @ $V_{BC} = 0$ and $V_{BE} >> v_{kT}$ as

$$I_{C(low-level)} \cong I_{SS}\exp\left(\frac{V_{BE}}{v_{kT}}\right) \quad (11.110)$$

At the transition point from the low-level injection to high-level injection, the collector current must be continuous and, therefore, equal. Let us assume that the intersection of high current and low current asymptote is given by (I_{KF}, V_{KF}) at $I_{C(high-level)} = I_{C(low-level)}$. Therefore, from Equations 11.109 and 11.110 at the transition point (I_{KF}, V_{KF}), we can show

$$I_{KF} = \sqrt{\frac{Q_{B0}I_{SS}}{\tau_f}}\exp\left(\frac{V_{KF}}{2v_{kT}}\right) \quad (11.111)$$

and

$$I_{KF} \cong I_{SS}\exp\left(\frac{V_{KF}}{v_{kT}}\right) \quad (11.112)$$

From the above equations, we can show that the collector current at the transition from the low-level to high-level injection, called as the forward *knee-current*, I_{KF} is given by

$$I_{KF} = \frac{Q_{B0}}{\tau_f} \quad (11.113)$$

Figure 11.26 shows the knee-point (I_{KF}, V_{KF}) in the $\ln(I_C)$ versus V_{BE} plot at $V_{BC} = 0$. It is observed from Figure 11.26 that the slope of $\ln(I_C) - V_{BE}/v_{kT}$ plot for high-level injection is, clearly, smaller (theoretically, about 1/2) than that due to low-level injection.

Similarly, we can show that in the *reverse mode* of BJT operation, the *inverse knee-current* I_{KR} is given by

$$I_{KR} = \frac{Q_{B0}}{\tau_r} \quad (11.114)$$

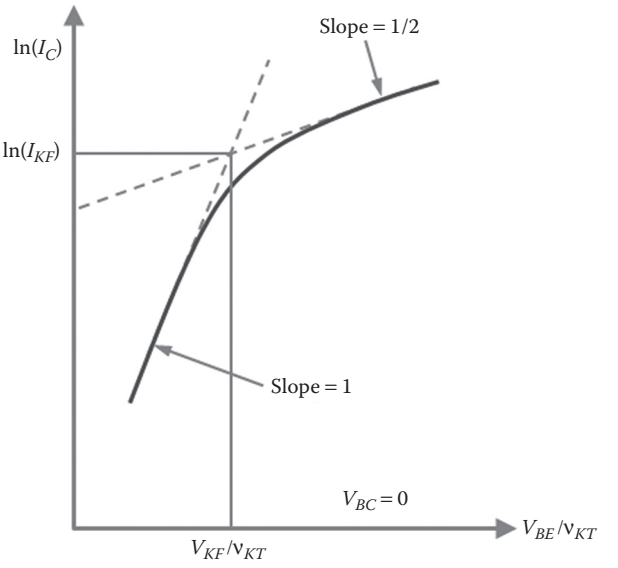

FIGURE 11.26
The forward ln(I_C) versus V_{BE}/v_{kT} plot of an *npn*-BJT: the plot shows the asymptotes of the low-level and high-level injections and the transition or knee-point (I_{KF}, V_{KF}) at the transition from the low-level to high-level injection.

Thus, the high-level injection in BJTs are modeled by forward and reverse knee-currents I_{KF} and I_{KR}, respectively, whereas the base-width modulation is modeled by the forward and reverse early voltages V_{AF} and V_{AR}, respectively.

The early effect and high-level injection model parameters (V_{AF}, V_{AR}, I_{SS}, I_{KF}, I_{KR}) are extracted from the following set of device characteristics.

- ln(I_C) versus V_{BE} plot at $V_{BC} = 0$ in the normal mode of BJT operation;
- ln(I_E) versus V_{BC} plot at $V_{BE} = 0$ in the inverse mode of BJT operation;
- I_C versus V_{CE} characteristics for different I_B (or V_{BE}) in the normal mode of BJT operation;
- I_E versus V_{EC} characteristics for different I_B (or V_{BC}) in the inverse mode of BJT operation.

11.5.5 Summary of Compact BJT Model

The complete set of BJT-model parameters consists of basic (EM1) dc parameters, EM2 model parameters for parasitic elements, space-charge layer recombination model parameters, and the unified integrated charge control

model parameters describing the base-width modulation and high-level injection. The complete set of parameters is summarized below:

- Basic (EM1) DC model parameters: $\{\beta_{FM}, \beta_{RM}, T_{ref}, E_g, I_{SS}\}$
- Parasitic elements model parameters for: bulk-ohmic resistors, $\{r_c, r_e, r_b\}$ and charge storage elements: $\{C_{jE0}, \phi_{BE}, m_{jE}, C_{jC0}, \phi_{BC}, m_{jC}, \tau_f, \tau_r, C_{sub}\}$
- Space-charge layer recombination model parameters for modeling low-current β degradation: $\{C_2, n_E, C_4, n_C\}$
- Base-width modulation and high-level injection parameters: $\{V_{AF}, V_{AR}, I_{KF}, I_{KR}\}$

The equivalent circuit of the final SGP BJT model described above is represented by Figure 11.27 with redefined saturation current I_{SS} (Equation 11.66) and current source I_{CT} to model the early effect and high-level injection. The expression for I_{CT} in the SGP BJT equivalent circuit in Figure 11.27 is given by Equation 11.69 as

$$I_{CT} = \frac{I_{SS}}{q_b}\left\{\left[\exp\left(\frac{V_{BE}}{v_{kT}}\right)-1\right]-\left[\exp\left(\frac{V_{BC}}{v_{kT}}\right)-1\right]\right\} \tag{11.115}$$

where the normalized base charge q_b is given by Equation 11.101. Again, the expressions for I_{EC} and I_{CC} are given by Equation 11.13. Then we can write the expressions for the terminal current in a BJT with reference to Figure 11.27.

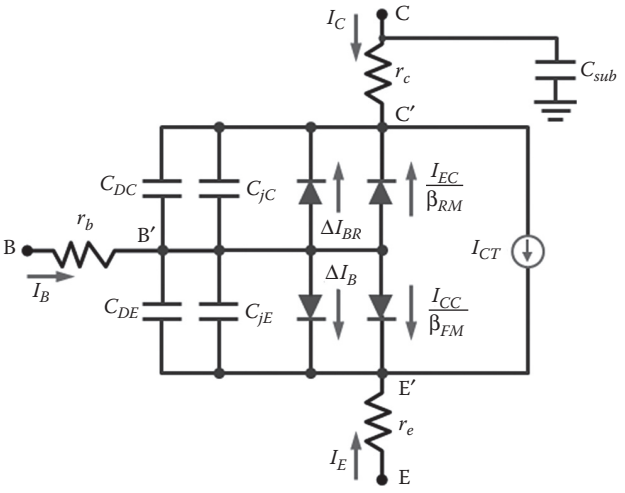

FIGURE 11.27
The equivalent circuit of SGP *npn*-BJT model: the current source I_{CT} is redefined to account for the base-width modulation and high-level injections.

With reference to Figure 11.27, the base current in SGP BJT model can be obtained from Equation 11.52 as

$$I_B = \frac{I_{SS}}{\beta_{FM}}\left[\exp\left(\frac{V_{BE}}{v_{kT}}\right)-1\right]+C_2 I_{SS}\left[\exp\left(\frac{V_{BE}}{n_E v_{kT}}\right)-1\right]+\frac{I_{SS}}{\beta_{RM}}\left[\exp\left(\frac{V_{BC}}{v_{kT}}\right)-1\right] + C_4 I_{SS}\left[\exp\left(\frac{V_{BC}}{n_C v_{kT}}\right)-1\right] \tag{11.116}$$

and the collector current is given by

$$I_C = \frac{I_{SS}}{q_b}\left[\exp\left(\frac{V_{BE}}{v_{kT}}\right)-\exp\left(\frac{V_{BC}}{v_{kT}}\right)\right]+\frac{I_{SS}}{\beta_{RM}}\left[\exp\left(\frac{V_{BC}}{v_{kT}}\right)-1\right] -C_4 I_{SS}\left[\exp\left(\frac{V_{BC}}{n_C v_{kT}}\right)-1\right] \tag{11.117}$$

The corresponding model equations as implemented in SPICE are as follows:

$$I_B = \frac{IS_{eff}}{\beta_F}\left[\exp\left(\frac{V_{BE}}{n_F v_{kT}}\right)-1\right]+ISE_{eff}\left[\exp\left(\frac{V_{BE}}{n_E v_{kT}}\right)-1\right] + \frac{IS_{eff}}{\beta_R}\left[\exp\left(\frac{V_{BC}}{n_R v_{kT}}\right)-1\right]+ISC_{eff}\left[\exp\left(\frac{V_{BC}}{n_C v_{kT}}\right)-1\right] \tag{11.118}$$

and,

$$I_C = \frac{IS_{eff}}{q_b}\left[\exp\left(\frac{V_{BE}}{n_F v_{kT}}\right)-\exp\left(\frac{V_{BC}}{n_R v_{kT}}\right)\right]-\frac{IS_{eff}}{\beta_R}\left[\exp\left(\frac{V_{BC}}{n_R v_{kT}}\right)-1\right] -ISC_{eff}\left[\exp\left(\frac{V_{BC}}{n_C v_{kT}}\right)-1\right] \tag{11.119}$$

Comparing derived Equations 11.116 and 11.117 with the SPICE implementation corresponding Equations 11.118 and 11.119, we find: $I_{SS} = IS_{eff}$; $C_2 I_{SS} = ISE_{eff}$; $C_4 I_{SS} = ISC_{eff}$; $\beta_{FM} = \beta_F$; and $\beta_{RM} = \beta_R$. In addition, the parameters n_F and n_R are included as the fitting parameters to improve the accuracy of data fitting with the model.

A complete set of SGP BJT compact model parameters is extracted from the following set of measurement data set for BJT parameter extraction including:

- Forward characteristics
  - Gummel plot (I_C, I_B) versus V_{BE} with $V_{BC} = 0$
  - I_C versus V_{CE}
  - Cut-off frequency, f_T versus I_C
- Reverse characteristics
  - Gummel plot (I_E, I_B) versus V_{EB} with $V_{BE} = 0$
  - I_E versus V_{CE}

The SGP model does not model the devices in the reverse mode as accurately as in the forward mode. Though BJTs are normally operated in the forward mode, both forward and reverse data are needed to extract series resistances.

In addition EB and CB *pn*-junction structures are used to extract capacitance model parameters $\{C_{j0}, \phi_{bi}, m_j\}$.

11.6 Summary

This chapter presented the basic BJT model for circuit simulation. A systematic methodology is presented to derive SGP BJT compact model starting from the basic EM model. An overview of the model parameter extraction is presented. The objective of this chapter is to expose readers to the basic understanding of BJT device modeling. The readers involved in BJT device engineering can extend the basic understanding from this study to more appropriate advanced BJT models.

Exercises

11.1 An *npn*-BJT is used as an open-collector *pn*-junction diode as shown in Figure E11.1. Then

a. Use the injection version of EM1 BJT model to derive an expression for the emitter current I_E as a function of V_{BE};

b. Use the expression derived in part (a) to calculate V_{BE} for $I_E = -1$ mA.

Given that: $\alpha_F = 0.98$; $\alpha_R = 0.49$; $I_{ES} = 10^{-16}$ A, and $T = 300$ K.

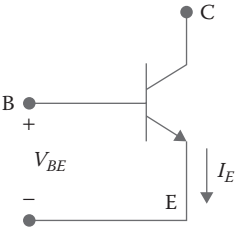

FIGURE E11.1
An open collector *npn*-BJT used as a two terminal EB *pn*-junction diode.

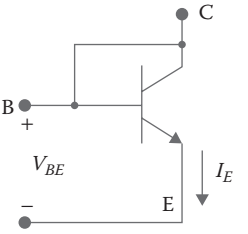

FIGURE E11.2
An *npn*-BJT is used as a two-terminal EB *pn*-junction diode with CB terminals shorted.

11.2 The *npn*-BJT in exercise 11.1 is used as a shorted base-collector diode as shown in Figure E11.2. Then use the parameters given in exercise 11.1 earlier to answer the following:

a. Use the injection version of EM1 BJT model to derive an expression for the emitter current I_E as a function of V_{BE}

b. Use the expression derived in part (a) to calculate V_{BE} for $I_E = -1$ mA

11.3 The basic (EM1) *npn*-BJT compact model is discussed in Section 11.5.1. Following the same procedure, develop the EM1 type model equations for a lateral *pnp*-BJT as shown in Figure E11.3.

a. Sketch the basic EM1 model; define and label all parameters.

b. Write equations for the terminal currents; define and explain all parameters.

c. If the *pnp*-BJT is used as a shorted base-collector diode, then from EM1 model equations in part (b) calculate the EB voltage at $I_E = 1$ mA. Given that: $I_{ES} = 10^{-16}$ A, $I_{CS} = 2.0 \times 10^{-16}$ A, $\alpha_F = 0.98$, $\alpha_R = 0.49$, and $T = 300$ K. Define and explain all parameters.

d. Include the bulk-ohmic resistors and charge storage elements to your model in part (a) to generate and sketch the lateral *pnp*-BJT EM2 model. Define and label all parameters.

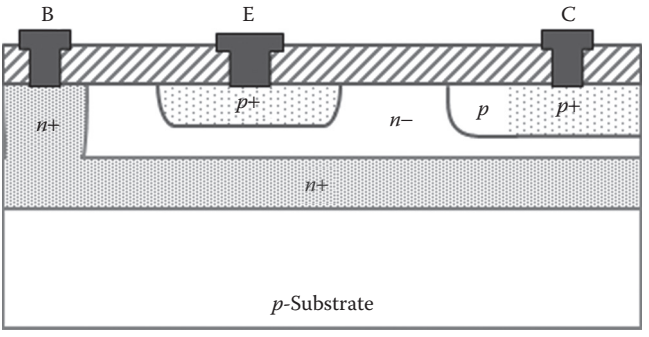

FIGURE E11.3
An ideal lateral *pnp*-BJT structure on a *p*-substrate: E, B, and C are the emitter, base, and collector terminals, respectively.

11.4 Consider an *npn*-BJT in the inverse active mode of operation in the high-level injection regime. For simplicity of modeling, you can assume uniformly doped base region.

a. Schematically show the components of base charge, Q_B, under the above operating condition. Label your plot and show the integration limits to compute different components of Q_B.

b. Write down the expression for the normalized base-charge responsible for base-width modulation in terms of junction biases and early voltages. Define all parameters and explain.

c. Write down the expression for SGP-model current source for base-width modulation in terms of early voltages only under the above specified operating condition. Define all parameters and explain.

11.5 The Gummel plot shown in Figure 11.20 for *npn*-BJT is obtained at $V_{BC} = 0$ and is used for DC compact model parameter extraction.

a. Describe graphically how I_C versus V_{BE} characteristics at $V_{BC} = 0$ can be obtained from I_C versus V_{CE} characteristics at different V_{BE} for an *npn*-BJT.

b. Mathematically describe the methodology to extract BJT saturation current I_{SS} for $I_C - V_{BE}$ plot at $V_{BC} = 0$.

Clearly define any assumptions you make.

11.6 The measured forward Gummel-plot of an *npn*-BJT is shown in Figure E11.4. Extract the following SGP-model parameters.

a. BJT saturation current, I_{SS}. Explain the extraction procedure.

b. Maximum forward current gain, β_{FM}. Explain the extraction procedure.

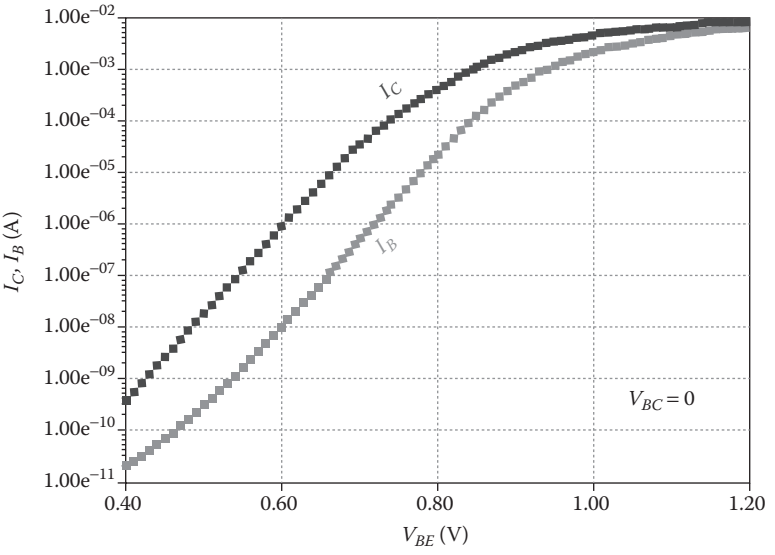

FIGURE E11.4
Measured forward Gummel plot of an *npn*-BJT used to extract SGP BJT device model parameters.

c. Forward "Knee" current, I_{KF}. Explain the extraction procedure.
d. The value of V_{BE} at $I_C = I_{KF}$. Explain the extraction procedure.
e. If the extracted forward transit time $\tau_f = 1$ ns, calculate the zero-bias base charge, Q_{B0} of the device.
f. Use the extracted value of Q_{B0} from part (e) to calculate the forward emission coefficient, n_E, that is, slope of $\ln(I_C)$ versus qV_{BE}/kT plot of the given characteristics at room temperature at the onset of high-level injection. Assume the width of the zero-bias neutral base region, $W_B = 0.2$ μm, $V_B = 10$ V, and area of the intrinsic BJT shown in Figure E11.4 is unity.

State any assumptions you make.

11.7 Consider a vertical *npn*-BJT operating in the normal active mode. The *p*-type base region is uniformly doped with concentration, $N_{aB} = 2.0 \times 10^{17}$ cm^{-3} and depth = 1.0 μm. The *n*-type emitter is formed by ion implantation with doping concentration, $N_{dE} = 2.0 \times 10^{20}$ cm^{-3} and depth = 0.3 μm. Neglect the space-charge recombination current for high-level injection to answer the following questions. Clearly define all parameters and explain.

a. What is the minority-carrier density in the *p*-base at which the high-level injection is reached?

b. Calculate the base-emitter forward bias V_{KF} at which the *high-level injection* is reached.

c. If the effect of *high-level injection* on the current gain β starts when the injected minority-carrier density reaches 10% of the majority carrier density, calculate the value of V_{BE} at the onset of β roll-off at high collector current level, I_C.

d. Show the conditions obtained in part (b) and (c) on I_C vs. V_{BE} @ $V_{BC} = 0$ characteristic of the transistor.

Define and label all parameters in your plot(s). Explain.

11.8 The SGP-BJT model, presented in this chapter, cannot model the effect of parasitic substrate transistor on intrinsic devices. Consider the 2D cross section of dual-poly *npn*-BJT with a parasitic vertical *pnp*-BJT with the *p*-base as the emitter as shown in Figure E11.5. In this problem, you will modify the intrinsic vertical *npn*-BJT SGP model to include the effect of parasitic *pnp*-BJT. Clearly, state any assumptions you make, define all parameters, and label all terminal currents.

a. Draw the SGP equivalent network for the parasitic vertical *pnp*-BJT shown in Figure E11.5.

b. Use block diagrams to include the parasitic *pnp*-BJT network and the base-emitter and base-collector overlap oxide capacitances into the intrinsic *npn*-BJT model.

11.9 The small signal base-collector junction capacitance, C_{jC} versus V_{BC}, characteristics of an *npn*-BJT is shown in Figure E11.6. From the figure, extract the following diode model parameters. Clearly state any model you use and explain the procedure for each case.

a. CB-junction capacitance, C_{jC0} at $V_{BC} = 0$.

b. Built-in potential, ϕ_{BC}.

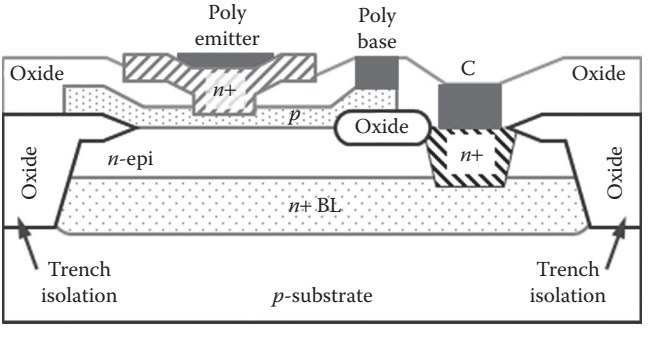

FIGURE E11.5
Trench isolated double polysilicon *npn*-BJT structure: poly emitter, poly base, and C represent emitter, base, and collector terminals, respectively.

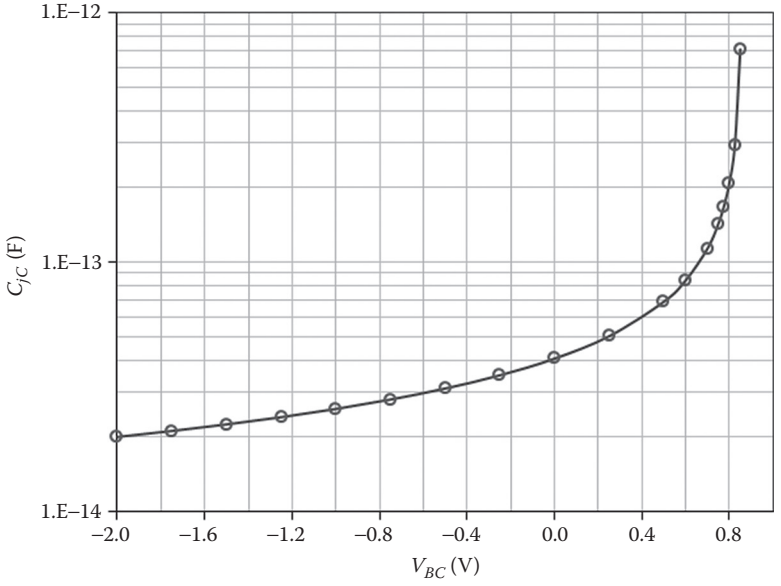

FIGURE E11.6
CB *pn*-junction *C*–*V* characteristics used to extract capacitance compact model parameters for *npn*-BJTs.

c. Calculate the junction gradient factor, m_{jC}.

d. If the integrated base charge, $Q_{B0} = 1.31 \times 10^{-12}$ C at $V_{BE} = V_{BC} = 0$, calculate the forward early voltage V_{AF} for the device operating in the normal active mode with CB-junction reverse biased at 2.0 V. Clearly state any assumptions you make.

11.10 A typical SGP *npn*-BJT compact model card of a typical bipolar technology is shown in Table E11.1. Consider an *npn*-BJT with emitter area, $A_E = 25$ μm² of this technology used in an integrated circuit to operate in the normal active mode at the biasing condition, $V_{BE} = 0.61$ V and $V_{CE} = 3$ V.

Use the relevant SGP model parameters from the given model card to answer the following questions. Define each parameter and explain your results. Assume that $V_{B'E'} = V_{BE}$ and $V_{B'C'} = V_{BC}$.

a. Calculate the base charge Q_{B0} in the neutral base region at $V_{BE} = 0 = V_{BC}$.

b. Calculate the normalized base charge q_1 that models the base-width modulation.

c. Calculate the normalized base charge, q_2 that models the high-level injection.

TABLE E11.1

A Typical SGP Model Card of an *npn*-BJT for Circuit Simulation

.option gmin = 1.0000000−16		
.model NPN1 npn (	LEVEL = 1	
+ bf = 2.1139717E+01	br = 4.9802084E+0	brs = 0.0000000E+00
+ Gamma = 0.0000000E+00	ikf = 2.3796255E–04	ikr = 1.0738911E–04
+ irb = 0.0000000E+00	is = 3.7746394E–18	isc = 3.4311697E–15
+ ise = 4.5630707E–15	nc = 1.9324214E+00	ne = 1.7137365E+00
+ Nepi = 1.0000000E+00	nf = 1.0000000E+00	nkf = 5.0000000E–01
+ nr = 1.0000000E+00	rb = 6.7165161E+02	rbm = 1.0000000E–01
+ rc = 9.9999998E–03	re = 4.8533592E+01	vaf = 4.3480446E+01
+ var = 6.0068092E+00	vo = 0.0000000E+00	cjc = 1.3075999E–15
+ cje = 3.8835999E–15	cjs = 0.0000000E+00	fc = 5.0000000E–01
+ itf = 3.2536294E–03	mjc = 1.4907001E–01	mje = 1.7038001E–01
+ mjs = 5.0000000E–01	ptf = 0.0000000E+00	qco = 0.0000000E+00
+ tf = 7.7961665E–11	tr = 0.0000000E+00	vjc = 1.0000000E–01
+ vje = 1.7466000E–01	vjs = 1.0000000E+00	vtf = 2.2093861E+00
+ xcjc = 1.0000000E+00	xtf = 3.4448984E+00	tref = 2.7000000E+01
+ eg = 1.1100000E+00	xtb = 0.0000000E+00	xti = 3.0000000E+00
+ subs = 1)		

Note: The parameters in the model card: $is = I_{SS}$; $ise = C_2 I_{SS}$; and $i_{SC} = C_4 I_{SS}$.

d. Calculate the total normalized base charge, q_b. From your results, what is your conclusion on the injection level under the biasing condition?

e. Calculate the base current I_B at the operating point.

f. Calculate the collector current I_C at the operating point.